SLEI3D: Simultaneous Exploration and Inspection via Heterogeneous Fleets under Limited Communication

Junfeng Chen[1], Yuxiao Zhu[2], Xintong Zhang[2], Bing Luo[2], and Meng Guo[1]

***Abstract*—Robotic fleets such as unmanned aerial and ground vehicles have been widely used for routine inspections of static environments, where the areas of interest are known and planned in advance. However, in many applications, such areas of interest are unknown and should be identified online during exploration. Thus, this paper considers the problem of simultaneous exploration, inspection of unknown environments and then real-time communication to a mobile ground control station to report the findings. The heterogeneous robots are equipped with different sensors, e.g., long-range lidars for fast exploration and close-range cameras for detailed inspection. Furthermore, global communication is often unavailable in such environments, where the robots can only communicate with each other via ad-hoc wireless networks when they are in close proximity and free of obstruction. This work proposes a novel planning and coordination framework (SLEI3D) that integrates the online strategies for collaborative 3D exploration, adaptive inspection and timely communication (via the intermittent or proactive protocols). To account for uncertainties w.r.t. the number and location of features, a multi-layer and multi-rate planning mechanism is developed for inter-and-intra robot subgroups, to actively meet and coordinate their local plans. The proposed framework is validated extensively via high-fidelity simulations of numerous large-scale missions with up to 48 robots and 384 thousand cubic meters. Hardware experiments of 7 robots are also conducted. Project website is available at https://junfengchen-robotics.github.io/SLEI3D/.**

***Note to Practitioners*—This paper is motivated by the challenges of coordinating large-scale heterogeneous fleets for the inspection of large buildings and infrastructure, where heterogeneous UAVs must collaborate to explore unknown environments, identify areas of interest, and more importantly, inspect specific features (such as cracks, leaks, and other anomalies). Furthermore, these features must be relayed back to a control station for further analyses. Existing methods predominantly focuses on exploration tasks and often overlooks the need for close-up inspection. Instead, a hierarchical and flexible framework is proposed to coordinate a group of heterogeneous UAVs online for efficient exploration, inspection and communication, subject to an unknown number and location of features. Instead of relying on an all-to-all communication network, limited communication range and bandwidth are addressed by leveraging intermittent and proactive communication protocols, i.e., to enable exchange of local plans, explored areas, and detected features during online execution. Via extensive simulations in a high-fidelity simulator, the proposed framework is shown to be efficient and reliable for large-scale simultaneous exploration and inspection tasks within various scenes. Robustness to robot failures and communication loss is also demonstrated. Hardware experiments over UGVs and UAVs validate the practical relevance.**

***Index Terms*—Heterogeneous multi-robot system, 3D exploration, collaborative task planning, intermittent communication.**

Received 20 January 2025; revised 30 March 2025; revised 04 November 2025; accepted 03 December 2025. This article was recommended for publication by Associate Editor Dr. Hytowitz, Rebecca upon evaluation of the reviewers' comments. This work was supported by the National Natural Science Foundation of China (NSFC) under grants U2241214, 62203017 and T2121002. (*Corresponding author: Meng Guo.*)

The authors are with [1]the School of Advanced Manufacturing and Robotics, Peking University, Beijing 100871, China; and [2]the Division of Natural and Applied Sciences, Duke Kunshan University, Suzhou 215316, China. meng.guo@pku.edu.cn

Digital Object Identifier (DOI): see top of this page.

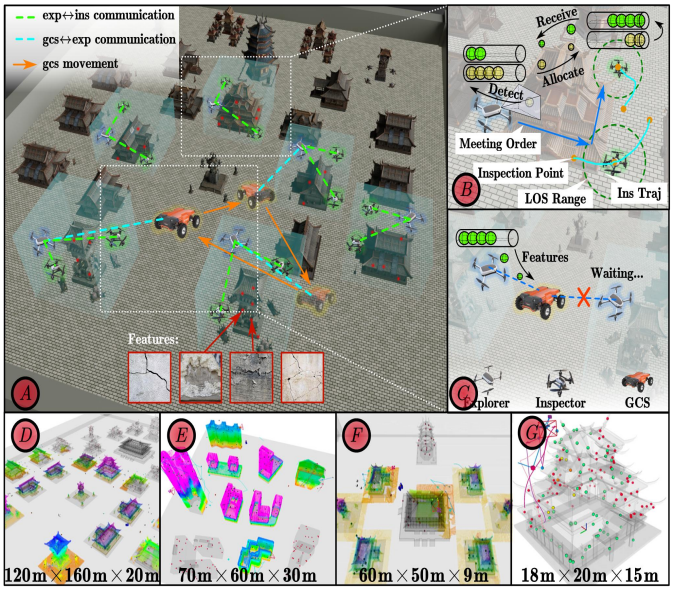

Figure 1: (a) 6 explorers and 12 inspectors are tasked to simultaneously explore and inspect an unknown number of numerous features; **(b)** the explorer and inspectors within the same subgroup coordinate for the inspection tasks; **(c)** the mobile ground station actively meets with the explorers to receive the latest features; **(d)-(g)** snapshots of online execution in four different large-scale scenes.

I. Introduction

Fleets of unmanned aerial vehicles (UAVs) and ground vehicles (UGVs) have been deployed to perform routine maintenance and inspection tasks for large and remote infrastructures such as power plants [1], bridges [2], [3] and industrial sites [4]. Such tasks are often static and repetitive, where the sequence of areas to visit and inspect are given in advance. However, in many applications as highlighted in Fig. 1, both the environment and the areas of interests (AoI) are unknown a priori, which requires the robots to simultaneously explore the environment, identify the AoI, and then inspect the features therein. Most existing work on collaborative exploration [5] has focused on only the exploration task to obtain the global map quickly, which overlooks the need for close-up inspection of certain features detected during exploration [6], e.g., cracks in planetary caves [7], life signs during search and rescue [8], and zoomed images at archaeological sites [9].

This article has been accepted for publication in IEEE Transactions on Automation Science and Engineering. This is the author's version which has not been fully edited and content may change prior to final publication. Citation information: DOI 10.1109/TASE.2025.3643166

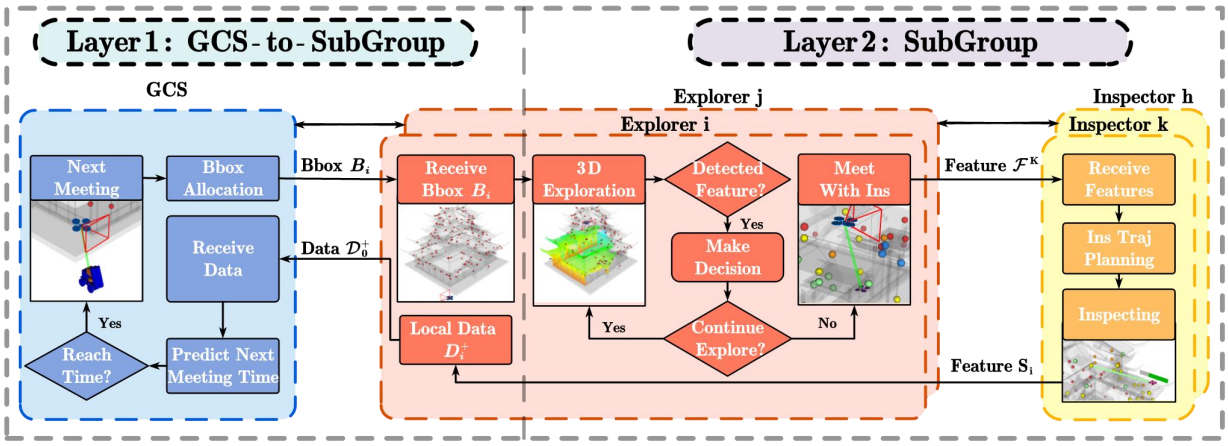

Figure 2: Overview of the proposed method, which consists of two hierarchical layers: the first layer where GCS coordinates with explorers, and the second layer where the explorer coordinates with inspectors within each subgroup, all under limited communication.

More importantly, these work often assumes a global all-to-all communication among the robots, which could be impractical in many aforementioned scenes where the communication facilities are unavailable [10] or severely degraded [11]. In such cases, the robots can only exchange information via ad-hoc networks subject to the line-of-sight (LOS) [12] and proximity constraints [13]. This imposes great challenges on the coordination of the robotic fleet as communication events, exploration and inspection tasks are now closely dependent, thus should be planned simultaneously [14].

Moreover, it is often essential to provide a timely update to a mobile ground control station (GCS), regarding the progress of exploration and inspected features, e.g., to plan for further actions such as maintenance and repair [15]. This can be particularly challenging without a global communication network, as the GCS would lose connection whenever the robots spread out for exploration [16]. In other words, the robots and the GCS should actively and frequently coordinate their communication including time, location and the content. How to design such a flexible and efficient coordination framework for the GCS and robotic fleets remains unsolved.

As shown in Fig. 2, this work proposes a simultaneous large-scale exploration, inspection and communication framework (SLEI3D) for a heterogeneous robotic fleet that operates in unknown environments under limited communication. Given the bounding boxes that enclose the AoI, the robots are divided into numerous subgroups of explorers and inspectors. As an essential component, a 3D collaborative exploration strategy is designed for explorers with long-range Lidars to detect AoI efficiently, based on geometric-aware frontier generation. Allocation of the identified AoI to inspectors with close-range cameras is then formulated as a 3D constrained routing problem, to maximize the inspection efficiency and ensure a safety distance. Then a prediction algorithm for the task completion time is designed for the GCS to rapidly collect the result of inspected features. More importantly, an intermittent communication protocol is designed between the GCS and the subgroups, to facilitate online data exchange and adaptation given the updated map and the features. In contrast, a proactive communication protocol is employed within each subgroup, where the explorer dynamically determines the time and location to communicate with the inspectors based on the detected features. The efficiency and reliability of the proposed framework are analyzed theoretically and validated via extensive large-scale simulations and hardware experiments. Up to 48 robots are deployed to explore and inspect numerous large-scale scenes with more than 150 inspection tasks.

Main contributions of this work are threefold: (I) the novel problem formulation of simultaneous exploration and inspection under limited communication for heterogeneous robotic fleets; (II) the multi-layer and multi-rate coordination framework that co-optimizes the exploration task, the inspection task and the inter-robot communication; and (III) the extensive large-scale simulations that validate the performance in practical scenes. To the best of our knowledge, this is the first work that provides such a comprehensive solution.

II. Related Work

A. Multi-robot Collaborative Exploration

Autonomous exploration has a long history in robotics [17], [18], e.g., [5] introduces an intuitive yet powerful frontier-based method for guiding the exploration. It has been adapted to multi-robot teams by assigning these frontiers to different robots for concurrent exploration via e.g., distributed auction [19], multi-vehicle routing [20], optimization of information gain in [21], and dynamic optimization of topological graph in [22]. On the other hand, the work in [23] presents a flooding algorithm that ensures multiple robots can explore the entire environment without missing any area. A multi-robot depth-first search (MR-DFS) method is proposed in [24] to explore unknown environments encoded as a graph by parallel search. However, these work commonly assumes that all robots can communicate instantly and exchange information at all times, i.e., they always have access to the same global map. However, this is often impractical for unknown environments where the inter-robot communication is limited in range. Besides the above classical methods, reinforcement learning (RL)-based approaches have also been applied to multi-robot exploration, see [25]. They mostly focus on the design of customized observation spaces encapsulating partial observability constraints and novel reward functions to improve exploration efficiency. Therefore, many recent work combines

the planning of inter-robot communication and autonomous exploration [26]. the work in [27] adopts fully-connected networks at all time, while radio dropplets are utilized in [28] as extended communication relays between robots. Nonetheless, these work considers only the task of collaborative exploration, without addressing the inspection tasks of certain features.

B. Autonomous Inspection

Autonomous inspection can already be found in various applications via different sensors, e.g., [8]. Such tasks involve generating a set of viewpoints based on the 3D structure and the sensor intrinsics, which are then assigned to the robots for inspection. A skeleton-based space decomposition method is proposed in [29] followed by a travel salesman problem (TSP) algorithm. The work in [30] generates via-points and path primitives using voxel dilation or subtraction, and employs a primitive coverage graph (PCG) to optimize the collective paths. However, these work primarily focuses on single-robot exploration strategies and is not directly applicable to multi-robot systems.

The work in [31] employs random sampling in combination with potential fields to generate candidate viewpoints, which are allocated to a fleet of UAVs by solving an integer optimization problem. Moreover, the Multi-UAV Coverage Path Planning for Inspection (MU-CPPI) algorithm in [32], addresses the allocation problem of viewpoints by formulating as a set-covering vehicle routing problem (SC-VRP). This approach builds on an *exploration-then-inspection* framework, where UAVs first fully explore the environment to construct a prior map, followed by dedicated inspection path planning based on the acquired data. This decoupling often leads to low efficiency of inspection. To tackle this, simultaneous exploration and photographing framework (SOAR) is proposed in [33], where SOAR employs LiDAR-equipped explorers to detect uncovered areas and generate inspection viewpoints at surface frontiers, while camera-equipped photographers are assigned to these viewpoints via solving a *Consistent Multiple Depot Multiple Traveling Salesman Problem* (Consistent-MDMTSP). However, it relies on the persistent all-to-all communication between UAVs and a static ground control station (GCS) for global task allocation. Furthermore, the framework designates a single explorer as the sole frontier detector, yielding a computational bottleneck in large-scale environments. The most relevant work [34] called CARIC, introduces a hierarchical strategy for simultaneous exploration and inspection in multi-robot systems. CARIC partitions robots into specialized teams assigned to subregions, where they perform local tasks and relay inspection results to a static GCS through line-of-sight (LOS) communication. However, CARIC enforces inter-robot connectivity by pre-defining communication points on rectangular bounding boxes, a method that cannot be applied to irregular bounding boxes with non-convex internal structures or to scenarios involving a dynamic GCS that interacts with multiple teams of heterogeneous UAVs.

C. Multi-robot Coordination under Limited Communication

The key challenge in multi-robot coordination under communication constraints, is to determine when and where inter-robot communication should occur, with the message content tailored to different purposes. This issue arises not only in cooperative exploration [35], but also in cooperative patrolling [36], and coverage planning [37]. Different communication protocols have been proposed, e.g., the work in [38] proposes the meeting-merging-mission protocol for all robots, by formulating a constrained integer optimization problem to determine the rendezvous points and the meeting time. In related work in [16] presents the protocol of distributed intermittent communication, by solving iteratively multiple vehicle routing problems with time window (MVRP-TW). The most relevant work [34] addresses the LOS communication constraints by choosing communication points on regular bounding boxes, which is not applicable to irregular structures. However, these work primarily assumes a uniform purpose.

III. Problem Description

A. Model of Workspace and Robots

Consider a group of N robots $\mathcal{N} \triangleq \{1, \cdots, N\}$ that collaborate in a common, unknown and bounded workspace $\mathcal{W} \subset \mathbb{R}^3$. It is assumed that the bounding size and shape of the workspace is known a priori. Each robot $i \in \mathcal{N}$ has a state $x_i \in \mathbb{R}^3$ and the system state is given by the stacked vector $X \triangleq [x_i] \in \mathcal{X}$. Due to the safety constraints such as inter-robot and robot-obstacle collision avoidance, the system state is restricted to a safety set $\widehat{\mathcal{X}} \subset \mathcal{X}$. There are two types of robots $\mathcal{N} \triangleq \mathcal{N}_{\mathrm{e}} \cup \mathcal{N}_{\mathrm{o}}$ with explorers $\mathcal{N}_{\mathrm{e}}$ and inspectors $\mathcal{N}_{\mathrm{o}}$. Each robot $i \in \mathcal{N}$ can perform SLAM locally and navigate within its map safely without colliding with other robots or detected obstacles. Denote by

$$\mathbf{p}_{sg} \triangleq \mathtt{Navi}_i(p_i,\, p_g,\, \mathcal{M}_i), \tag{1}$$

as the navigation module [39] that guides robot i from its current pose $p_i \in \mathcal{W}$ to a target pose $p_g \in \mathcal{W}$ via the path $\mathbf{p}_{sg}$ within its local workspace map $\mathcal{M}_i$, while ensuring that $\mathbf{p}_{sg} \subset \widehat{\mathcal{X}}$. Each pair of robots can exchange data via ad-hoc wireless communication networks, subject to the line-of-sight (LOS) and limited-range constraints. Denote by

$$(D_i^+,\, D_j^+) \triangleq \mathtt{Comm}_{ij}(D_i,\, D_j), \tag{2}$$

as the communication module that robots $i, j \in \mathcal{N}$ update their local data D_i and D_j via communication if their LOS is not blocked by obstacles in $\mathcal{W}$, and their relative distance is within their communication range, denoted by $r_{ij} > 0$.

In addition, there is a mobile GCS which has a unique index 0, which is only responsible for sending and receiving data and does not undertake the role of communication manager. It follows the same navigation module in (1), and has the same communication constraints with other robots in (2), i.e., the communication range is given by $r_{0i} > 0$, $\forall i \in \mathcal{N}$. Similarly, the local map at the GCS is denoted by $\mathcal{M}_0$ and local data by D_0, For brevity, denote by $\mathcal{N}^+ \triangleq \{0\} \cup \mathcal{N}$.

B. Exploration and Inspection

Each explorer $i \in \mathcal{N}_{\mathrm{e}}$ can update its local map via the exploration module

$$\mathcal{M}_i^+ \triangleq \mathtt{Explore}_i(p_i,\, \mathcal{M}_i,\, \mathcal{W}), \tag{3}$$

where $\mathcal{M}_i^+$ is the updated local map. For instance, the octomap [40] can be constructed online via lidars. Moreover, there are $Q > 0$ features of interest in the workspace, denoted by $\mathcal{F} \triangleq \{f_q, \forall q \in Q\}$. Given the updated map, each explorer $i \in \mathcal{N}_\text{e}$ can identify a set of potential Areas of Interest (AoI) in its local map that contains several features, through a perception system that integrates 3D reconstruction from fused visual-depth images, enhanced by real-time semantic segmentation and accelerated object detection [41], [42]. This detection process is formalized via the feature fusion module:

$$\big\{(f_q, \phi_q)\big\} \triangleq \texttt{Fit}_i(\mathcal{M}_i), \tag{4}$$

where $\phi_q \subset \mathcal{M}_i$ is the AoI that might contain feature $f_q \in \mathcal{F}$.

Each inspector $i \in \mathcal{N}_\circ$ can inspect an AoI ϕ_q in close range, i.e., to further determine whether the feature f_q exists within ϕ_q and its state, via the inspection module:

$$(D_i^+, s_q, t_q) \triangleq \texttt{Inspect}_i(p_i, f_q, \phi_q), \tag{5}$$

where $s_q \in \mathbb{R}^L$ is the grounded representation of feature f_q with dimension $L > 0$, such as positions, images and point clouds; $t_q > 0$ is the duration of inspecting feature f_q; and the local data D_i^+ is updated with the inspection results.

The GCS is required to collect data from the robotic fleet regarding the progress of exploration and inspection. The data collection process follows the same communication protocol as in (2) to update its local data D_0.

Example 1. As shown in Fig. 1, the archaeological mission considered in the simulation deploys 6 large UAVs as explorers with high-resolution Lidar to construct the global map of the entire site; 12 small UAVs as inspectors with cameras to take close-up images of numerous potential features; and 1 GCS to gather, coordinate and update features from the fleet. ■

C. Problem Formulation

The local plan of each robot $i \in \mathcal{N}^+$ is given by a sequence of navigation and various actions, i.e.,

$$\xi_i \triangleq \mathbf{p}_i^1 a_i^1 \cdots \mathbf{p}_i^t a_i^t, \tag{6}$$

where $\mathbf{p}_i^t \in \mathcal{W}$ is the sequence of waypoints; and a_i^t is the sequence of actions, i.e., exploration or communication for explorers $i \in \mathcal{N}_\text{e}$; inspection or communication for inspectors $i \in \mathcal{N}_\circ$ and communication for the GCS. The planning objective is to design the exploration, inspection and communication strategy for the robotic fleet, such that the total time of gathering all features by the GCS is minimized, i.e.,

$$\begin{aligned}
&\min_{\{\xi_i\}} \quad T \\
\textbf{s.t.} \quad &\mathcal{W} \subseteq M_0(T); && \text{(7a)}\\
&s_q \subseteq D_0(T),\ \forall q \in Q; && \text{(7b)}\\
&x(t) \in \widehat{\mathcal{X}},\ \forall t \in [0, T]; && \text{(7c)}\\
&(1) - (5),\ \forall i \in \mathcal{N}; && \text{(7d)}
\end{aligned}$$

where $T > 0$ is the duration of the mission to be minimized; the constraint (7a) ensures that the local map M_0 of the GCS at time $t = T$ contains the entire workspace; the constraint (7b) requires that the inspection results of all features within the entire workspace are obtained in the local data $D_0(T)$ of the GCS; and the other constraints (7c), (7d) ensure that the fleet follows the navigation, exploration, inspection and communication modules as described earlier.

IV. Proposed Solution

A. Overview of Proposed Method

The proposed method tackles above optimization problem in (7) via a multi-layer and multi-rate coordination framework that simultaneously co-optimizes the collaborative behaviors of GCS, explorers and inspectors. As illustrated in Fig. 2, the robotic exploration efficiency is enhanced by constraining the search space with prior knowledge regarding the distribution of AoI: bounding boxes $\mathcal{B} \triangleq \{B_i\} \subset \mathcal{W}$ that encapsulate clusters of internal architectures. However, this framework can also be applied to fully unknown workspace without any prior information, via a prior-free exploration module described in the sequel. Given BBoxes, the GCS is responsible for receding-horizon allocation of bounding boxes (BBoxes) denoted as $\mathcal{B} \triangleq \{B_1, B_2, \cdots\} \subset \mathcal{W}$, reassigning the subgroup to other unfinished BBoxes, and collecting both map information $\mathcal{M}$ and inspection results of features $\mathcal{S} \triangleq \{s_1, s_2, \cdots\}$. Initially, GCS divides all robots into multiple subgroups based on the number of explorers, BBoxes and the robotic sensing capabilities. Then, each subgroup is assigned to the nearest BBox using rolling assignment algorithm as described in the sequel. Furthermore, the proposed method adopts a two-layer communication structure, i.e., the first layer coordinates the GCS and subgroup at a low frequency, while the second layer manages the intra-group collaboration in higher frequency.

1) Layer of GCS-to-SubGroups: As for the GCS-to-SubGroup layer, an intermittent communication protocol is designed to facilitate the coordination between GCS and explorers, mainly focusing on three aspects: (I) Management of BBoxes. The GCS informs the location of BBoxes to the explorer of the subgroup, and explorer reports the completion status of BBoxes back to GCS. The rolling assignment algorithm is applied by GCS to assign any remaining BBoxes to the nearest subgroup to accelerate overall mission. (II) Collection of inspection results. Inspectors transmit their inspection results $\mathcal{S}$ to the explorer, which then forwards these results to GCS along with the exploration map $\mathcal{M}$. (III) Coordination of meeting time and location. GCS and the explorer negotiate the time and location of their next meeting by utilizing the prediction algorithm for task completion time. To further quantify the efficiency of task execution, the metrics to measure idle time associated with GCS and explorers are introduced. Specifically, τ_0 denotes the time GCS spends waiting to meet the explorer. For each explorer $i \in \mathcal{N}_\text{e}$, the idle time is defined as $\tau_i \triangleq \tau_i^- \cup \tau_i^+$, where τ_i^- denotes the travel time to the meeting location with GCS or the inspectors, and τ_i^+ is the waiting time at the meeting location before the meeting starts. Detailed descriptions are given in Sec. IV-B.

2) Layer of SubGroups: A proactive communication protocol within a subgroup is proposed to coordinate the collaboration between explorer and inspectors, under limited communication. It contains two main components: (I) Allocation

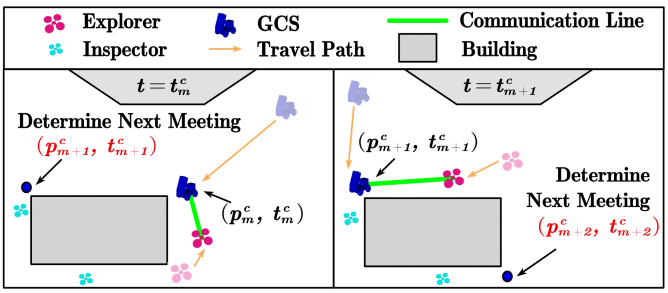

Figure 3: Intermittent communication between GCS and explorers.

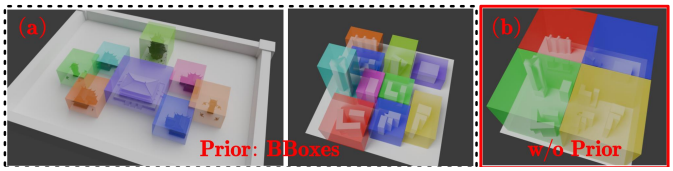

Figure 4: BBoxes Construction via the vertical buildings (**left**) for two scenarios; Adaptive BBox partition without any priors (**right**).

of AoIs. The explorer assigns detected AoIs to the inspectors. (II) Planning for inspection trajectories and relaying inspection results. Inspectors relay their inspection results and their planned trajectories to the explorer, to coordinate their next meeting events. To evaluate the efficiency of this intra-group coordination, the idle time $\tau_j \triangleq \tau_j^- \cup \tau_j^+$ is introduced as the efficiency metrics for each inspector $j \in \mathcal{N}_\circ$, where τ_j^- is the idle period when no features are available for inspection, and τ_j^+ is the travel time to the features.

Given the above multi-layer framework and the coordination strategies, the original problem in (7) is reformulated to minimize the total idle time of all robots, subject to the same constraints, i.e., the objective function is re-stated as follows:

$$\mathbf{min}_{\{\xi_i\}}\Big\{\sum_{i\in\mathcal{N}^+}\tau_i\Big\}, \tag{8}$$

where τ_i is the idle time for each robot $i \in \mathcal{N}^+$ as defined above. Note that minimizing T in (7) can be achieved by minimizing the total idle time, i.e., maximizing the mission efficiency for exploration, inspection and communication.

B. Layer of GCS-to-SubGroups

1) Subproblem Formulation: To ensure data collection online, the GCS and subgroups are required to meet and communicate frequently via an intermittent communication protocol under the communication module $\texttt{Comm}_{0i}, i \in \mathcal{N}_\text{e}$ in (2). Denote by $\mathcal{C} \triangleq C_1C_2\cdots$ the sequence of communication events, where $C_m = (p^\text{c}_m, t^\text{c}_m)$ represents the m-th communication between GCS and the explorers within each subgroup; p^c_m and t^c_m are the location and time for the m-th communication. Then, the protocol of intermittent communication is as follows: (I) GCS can communicate with the explorers when they satisfy the LOS and communication range; (II) during each communication, they determine locally the next meeting time and location. Then they depart and do not communicate until the next meeting. This procedure is repeated until termination, as shown in Fig. 3. Under this protocol, the idle time τ_i of the explorers $i \in \mathcal{N}_\text{e}$ mainly originates from the travel time $\tau_{i_m}^-$ from exploration to the meeting location p^c_m at the predefined time t^c_m, and the waiting time $\tau_{i_m}^+$ for the GCS. On the other hand, the idle time τ_{0_m} of the GCS is the waiting time for the explorer to arrive at p^c_m for the m-th communication. Therefore, the objective in (8) is to minimize the total idle time for explorers and GCS.

Problem 1. Determine the optimal plan $\{\xi_i, i \in \{0\} \cup \mathcal{N}_\text{e}\}$ such that the total idle time for the explorers and GCS is minimized, i.e., $\mathbf{min}_{\{\xi_i\}} \sum_{m=1}^{M}(\sum_{i\in\mathcal{N}_\text{e}} \tau_{i_m} + \tau_{0_m})$, where $M > 0$ is a predefined planning horizon as the number of communication rounds ahead. ■

To tackle Problem 1, a parametric method for BBoxes construction is proposed, as illustrated in Fig. 4 (a). For each building, its principal axis-aligned footprint $B_i^{\mathcal{F}} \subset \mathbb{R}^2$ is extracted from prior structural data or low-resolution scans. This footprint is then extruded vertically with a safety margin $\delta_z \in [\delta_{\min}, \delta_{\max}]$ to form the cubic bounding box $B_i \triangleq B_i^{\mathcal{F}} \times [z_{\texttt{base}} - \delta_z, z_{\texttt{top}} + \delta_z]$, where $z_{\texttt{base}}$ and $z_{\texttt{top}}$ denote the structure's elevation bounds. The complete search space is defined as $\mathcal{B} \triangleq \bigcup_{i=1}^{N} B_i \subset \mathcal{W}$, effectively encapsulating all surface-adjacent subspaces within ϵ-neighborhoods of building envelopes. This construction enables robotic fleets to execute surface-normal trajectory planning while avoiding computationally prohibitive full 3D reconstructions. For scenarios lacking prior structural knowledge, the system initiates an adaptive bounding box generation process, as detailed in Section IV-E5. Then, a predictor for task completion time is first proposed to estimate the time needed for the explorers to explore each BBox $B_i \in \mathcal{B}$, such that GCS can schedule the next communication event. Then, an exploration algorithm named $\texttt{FF3E}(\cdot)$ is proposed for the explorers to arrive at the meeting location p^c_m at time t^c_m, thereby minimizing the waiting time τ_0. Lastly, an algorithm is proposed for the GCS to coordinate the communication events with the explorers, to reduce the waiting time τ_i^+.

2) Prediction of Task Completion Time and Planning for Next Communication Event: An explorer $i \in \mathcal{N}_\text{e}$ first explores for a user-defined time $t^\text{e}_{i_m} < E_i$, during which it fits a set of features $\mathcal{F}_{i_m}$ by (4), and receives the inspection results of features $\mathcal{S}_{i_m}$. Then, explorer i estimates the time needed to complete the exploration of the entire BBox B_i, which serves as the next communication time t^c_{m+1}, i.e., the predictor for task completion time as follows:

$$t^\text{c}_{m+1} = \left(\frac{V_{B_i}}{|\mathcal{S}_{i_m}|}\right) \cdot \left(\frac{|\mathcal{F}_{i_m}|}{V^m_{B_i}}\right) \cdot t^\text{e}_{i_m}, \tag{9}$$

where $\mathcal{S}_{i_m} \subset \mathcal{S}$ is the set of inspection results, received by explorer i during the m-th communication; $V_{B_i} > 0$ is the total volume of BBox B_i, while $V^m_{B_i}$ represents the volume that has been explored by explorer i by the m-th communication. If no features are received, i.e., $\mathcal{S}_{i_m} = \varnothing$, the communication time $t^{\texttt{ideal}}_{m+1}$ is approximated by the ratio of explored volume, i.e., $V_{B_i} t^\text{e}_{i_m} / V^m_{B_i}$. In addition, the location p^c_{m+1} is chosen among the four corner points of the BBox B_i to the current location of explorer i, such that the estimated arrival time by the $A^\star$ algorithm following the navigation module $\texttt{Navi}(\cdot)$ in (1) is closest to the newly planned communication time t^c_{m+1}. Note that other prediction algorithms

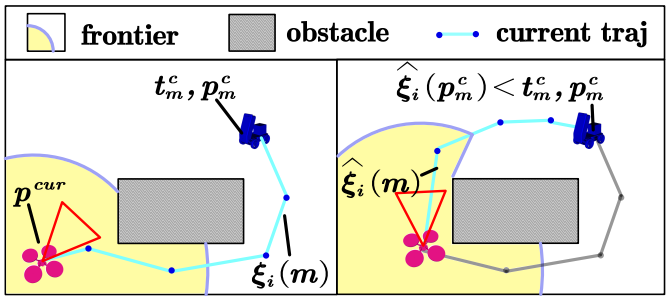

Figure 5: Fast frontier-based exploration and local adaptation of the exploration strategy $\{\mathbf{p}_i^t\}$ by the explorer.

than (9) can be integrated into the proposed framework, e.g., regression of existing data.

Remark 1. Different from the work [16] where the GCS communicates with all explorers in every round, the proposed method schedules communications based on the predicted time of task completion, thus eliminating the need for the GCS to communicate with all explorers in a predefined order. ■

3) Fast Frontier-based 3D Exploration: With a slight abuse of notation, the current local *plan* of explorer i is given by:

$$\xi_i(m) \triangleq \mathbf{p}_i^1 a_i^1 \cdots \mathbf{p}_i^t a_i^t \cdots p_m^c a_i^m, \quad t \leqslant t_m^c, \tag{10}$$

where p_m^c, t_m^c are the *confirmed* m-th communication between the GCS and explorer i; a_i^m is the communication action with GCS; and $\mathbf{p}_i^t, a_i^t$ are the waypoints and actions of exploration, which should be optimized to maximize the explored workspace within the communication time t_m^c. As illustrated in Fig. 5, More specifically, denote by $\widehat{\xi}_i(m) \triangleq \widehat{\mathbf{p}}_i^1 a_i^1 \cdots \widehat{\mathbf{p}}_i^t a_i^t \cdots \widehat{\mathbf{p}}_m^c a_m^c$ as the revised local plan, where $\{\widehat{\mathbf{p}}_i^t\}$ are the updated waypoints and $\widehat{\mathbf{p}}_m^c$ are the newly-added waypoints to the meeting location p_m^c. Thus, the waiting time for explorer i is given by $\tau_i^+ = \widehat{\xi}_i(p_m^c) - t_m^c$, where $\widehat{\xi}_i(p_m^c)$ is the estimated time of arriving at p_m^c.

Problem 2. Determine the local plan $\widehat{\xi}_i(m)$ such that: (I) the explored area is maximized within the communication time t_m^c; (II) the waiting time τ_i^+ is minimized. ■

To begin with, it is worth noting that these two objectives above are often conflicting. Existing algorithms [43] based on TSP or TSP-TW can not be directly applied as not all frontiers have to be visited. Therefore, the proposed solution under the module `Explore`$(\cdot)$ in (3) is summarized in Alg. 1. At each round m, explorer i first checks whether it has enough time t_m^c to reach the meeting location p_m^c in Lines 14-16. If $T' > 0$ does not hold, then $\varnothing$ is returned in Line 20. Otherwise, the algorithm proceeds to find the optimal waypoints $\widehat{\xi}_i^\star$ via the function `planPath`$(\cdot)$ in Line 18-19. More specifically, it checks if the total time spent plus the time needed to reach p_m^c exceeds the agreed meeting time t_m^c in Line 18. If so, this function returns the current path $\widehat{\xi}'$ in Line 3. Otherwise, it initializes the optimal path $\widehat{\xi}^\star$ as the current path $\widehat{\xi}'$ in Line 4. Then, it iterates through each frontier $P \in \Gamma$ in Line 5, by computing the distance D and the travel time $T_{p_0}^P$, from its position p_0 to P in Lines 6-7. Afterwards, the set of visited

Algorithm 1: Fast Frontier-based 3D Exploration: `FF3E`$(\cdot)$

Input: Current position p_i, Frontiers set Γ, Meeting location p_m^c, Meeting time t_m^c, Robot speed v_i
Output: Optimal path $\widehat{\xi}_i^\star$

1 **Function** `planPath`$(p_0,\ \widehat{\xi}',\ T^+)$**:**
2 **if** $T^+ + T_{p_k^c} > t_k^c$ **then**
3 **return** $\widehat{\xi}'$;
4 $\widehat{\xi}^\star \leftarrow \widehat{\xi}'$;
5 **for** *each point* $P \in \Gamma \backslash \widehat{\xi}'$ **do**
6 $D \leftarrow$ `GetDistance`$(p_0,\ P)$;
7 $T_{p_0}^P \leftarrow D / v_i$;
8 $\widehat{\xi}' \leftarrow \widehat{\xi}' + [P]$;
9 $T^+ \leftarrow T^+ + T_{p_0}^P$;
10 $\widehat{\xi}^+ \leftarrow$ `planPath`$(P, \widehat{\xi}', T^+)$;
11 **if** $dist(\widehat{\xi}^+) > dist(\widehat{\xi}^\star)$ **then**
12 $\widehat{\xi}^\star \leftarrow \widehat{\xi}^+$;
13 **return** $\widehat{\xi}^\star$;
14 $D_m^c \leftarrow$ `GetDistance`$(p_i,\ p_m^c)$;
15 $T_{p_m^c} \leftarrow D_m^c / v_i$;
16 $T' \leftarrow t_m^c - T_{p_m^c}$;
17 **if** $T' > 0$ **then**
18 $\widehat{\xi}_i^\star \leftarrow$ `planPath`$(p_i, [], 0)$;
19 $\widehat{\xi}_i^\star \leftarrow \widehat{\xi}_i' + [p_m^c]$;
20 **return** $\widehat{\xi}_i^\star$;

frontiers $\widehat{\xi}'$ is updated along with the total time spent T^+, before calling `planPath`$(\cdot)$ again in Line 10. Lastly, if the resulting path $\widehat{\xi}^+$ is longer than $\widehat{\xi}^\star$, the optimal path $\widehat{\xi}_i^\star$ is updated accordingly in Lines 11-12. Lastly, $\widehat{\xi}_i^\star$ from Alg. 1 is returned as the optimized solution for Problem 2.

The time complexity of Alg. 1 can be analyzed step by step based on its recursive structure. During initialization in Lines 14- 16, it mainly computes the distance and time to reach the meeting location p_m^c, thus the complexity is $\mathcal{O}(1)$. Then, during the recursive path planning, function `planPath`$(\cdot)$ explores all possible frontier points $P \in \Gamma$ by calling itself recursively in Line 10. The worst-case time complexity is $\mathcal{O}(|\Gamma|!)$, where $|\Gamma|$ is the total number of frontiers. Lastly, to update the optimal path in Line 3 has a complexity of $\mathcal{O}(1)$. Therefore, the overall complexity of Alg. 1 is given by $\mathcal{O}(|\Gamma|!)$.

4) Communication Coordination for GCS: To minimize the idle time τ_0 for GCS, it is sufficient to arrive at the meeting location p_m^c within the predefined time t_m^c. Therefore, a TSP-TW problem is formulated for GCS to optimize the sequence of meetings with the explorers in each communication $m \in M$. Detailed description is omitted due to limited space. In summary, the subproblem of coordinating GCS and explorers to minimize the idle time τ_i and τ_0 is solved by the proposed prediction algorithm of task completion time, 3D exploration algorithm and the intermittent communication protocol. It is worth noting that our framework does not require explicit calibration of the global localization between the GCS and explorers, via external positioning systems such as GPS or RTK. In addition, any pre-calibrated 3D coordinate in the

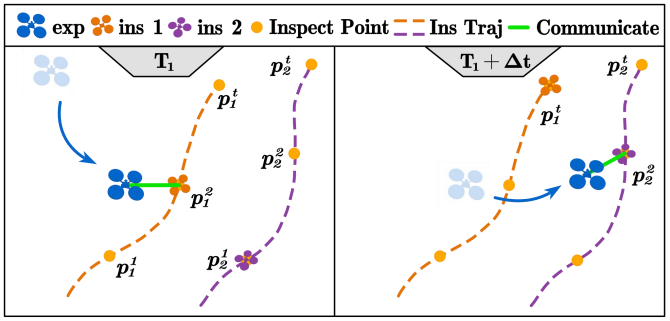

Figure 6: Proactive communication between an explorer (in blue) and the inspectors (in yellow) within a subgroup.

exploration area could serve as absolute references for GCS-to-explorer communications without additional calibration.

Lemma 1. *Under the proposed coordination strategy for the layer of GCS-to-SubGroups, all features $\mathcal{F}$ in the BBoxes can be fitted by explorers in finite time, of which the results can be collected by the GCS in finite time.*

Proof. During exploration, the explorers explore and fit features $\mathcal{F}_{i_m}$ via Alg. 1. The planning module $\texttt{planPath}(\cdot)$ in Line 1 ensures that all frontiers within a BBox B_i are visited and the whole BBox is fully explored. Since the number of frontiers $|\Gamma|$ in each BBox is finite, the total time required to explore any BBox is also limited. Furthermore, all BBoxes can be fully explored by the explorers via the rolling assignment algorithm. Thus, all features $\mathcal{F}$ in the environment can be fitted in finite time. On the other hand, the communication protocol schedules the next communication event $(p_m^{\mathrm{c}}, t_m^{\mathrm{c}})$, for which the explorers would adhere by Line 17. Similarly, the GCS ensures a timely arrival at the meeting event via solving the TSP-TW problem. During each communication, explorers can transmit all detected features to GCS. Since both the number of features and communication rounds are finite, the GCS can collect all results in finite time. ■

C. Communication-aware Exploration and Inspection

To minimize the idle time within the subgroup, a simultaneous exploration and inspection algorithm is proposed under the limited communication conditions.

1) Subproblem Formulation: Different from the scheme of intermittent communication, a novel proactive communication protocol under the module $\texttt{Comm}_{ij}(\cdot)$ in (2), is designed for the explorer $i \in \mathcal{N}_{\mathrm{e}}$ and the inspectors $\mathcal{N}_{\circ}^i \triangleq \{1, \cdots, K\} \subset \mathcal{N}_{\circ}$ within the subgroup. The protocol has two steps: (I) the explorer i communicates with the inspectors in $\mathcal{N}_{\circ}^i$ under the LOS constraints; (II) during each communication, the explorer determines not only the time and location of the next meeting with the inspectors under the energy constraint, but also assigns the fitted features to the inspectors. i.e., the features $\widehat{\mathcal{F}}_j \subset \mathcal{F}$ to inspect and the accordingly updated local plan ξ_j^+ of each inspector $j \in \mathcal{N}_{\circ}^i$. As illustrated in Fig. 6, this procedure is repeated until all features are fitted and inspected.

Definition 1 (Plan of Subgroup)**.** The overall plan of the subgroup is defined as a 4-tuple:

$$\Xi_i \triangleq (\widehat{\mathcal{N}}_i,\, \mathbf{c}_i,\, \boldsymbol{\varphi}_i,\, \boldsymbol{\xi}_i), \tag{11}$$

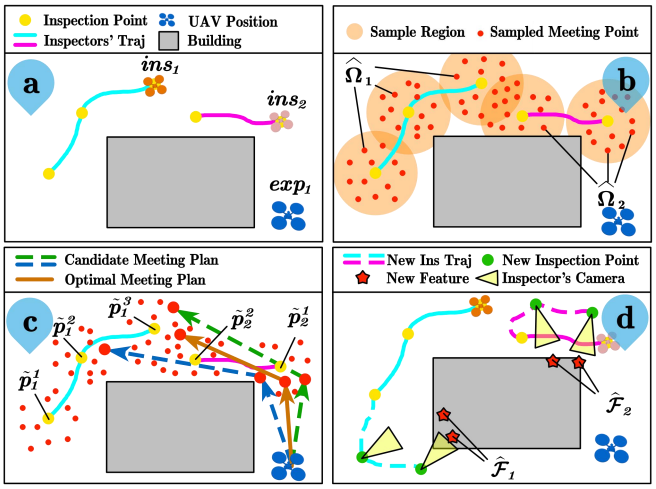

Figure 7: Main components of the proposed SOEI algorithm in Alg. 2: (**a**) the initialization of a subgroup including the explorer (in blue) and the inspectors (in yellow); (**b**) the sampling of candidate meeting locations $\{p_j\}$ (in red); (**c**) the optimization of meeting sequence $\mathbf{c}_i$ including meeting time and locations (in brown); and (**d**) the allocation of fitted features $\mathcal{F}_i^+$ (in red stars) to the inspectors $\widehat{\mathcal{N}}_i$.

where $\widehat{\mathcal{N}}_i \subset \mathcal{N}_{\circ}^i$ is the subset of inspectors to communicate with; $\mathbf{c}_i \triangleq \{(t_j, p_j), \forall j \in \widehat{\mathcal{N}}_i\}$ is the set of meeting time and location for each inspector in $\widehat{\mathcal{N}}_i$; $\boldsymbol{\varphi}_i \triangleq \{\widehat{\mathcal{F}}_j, \forall j \in \widehat{\mathcal{N}}_i\}$ is the set of new features allocated to each inspector, given the set of fitted features $\mathcal{F}_i^+$; and $\boldsymbol{\xi}_i \triangleq \{\xi_j^+, \forall j \in \widehat{\mathcal{N}}_i\}$ is the set of updated local plans for all inspectors. ■

Problem 3. Determine the plan of the subgroup Ξ_i as defined in (11) such that the total idle time of the explorer and inspectors within the subgroup is minimized, namely:

$$\min_{\Xi_i} \Big\{ \tau_i + \sum_{j \in \mathcal{N}_{\circ}^i} (\tau_j^+ + \tau_j^-) \Big\}, \tag{12}$$

where τ_j^+ is the idle time of inspector $j \in \mathcal{N}_{\circ}^i$ due to waiting; and τ_j^- is the remaining idle time excluding τ_j^+. ■

2) Efficient 3D Exploration and Inspection under Limited Communication: An efficient exploration and inspection algorithm encapsulated as $\texttt{SOEI}(\cdot)$ is proposed to solve the above problem. As illustrated in Fig. 7 and summarized in Alg. 2, it consists of three main parts as described in the sequel.

(I) Choice of inspectors. The optimal subgroup solution $\Xi_i^\star$ and the idle time $\tau_{\Xi^\star}$ are initialized in Line 1. Then, the algorithm iterates over each subset $\widehat{\mathcal{N}}_i \subset \mathcal{N}_{\circ}^i$, in order to evaluate the associated idle time. Note that if no inspectors are selected, the explorer would continue exploration. (II) Meeting Sequence. A sampling-based algorithm is proposed to determine the optimal sequence of meeting events between the explorer and the inspectors in $\widehat{\mathcal{N}}_i$. A set of sample points $\widehat{\Omega}_j$ are generated around the executing local plan $\{\xi_j^-\}$ of each inspector, subject to the LOS and range communication constraints. Denote by $\widehat{\mathbf{c}}' \triangleq \{\mathbf{c}_i'\}$ a set of potential sequences of meeting events, where each $\mathbf{c}_i'$ is formed by selecting one sample from $\widehat{\Omega}_j$ for each inspector and traversing the samples in a timed order. Afterwards, the optimal trajectory for the explorer to visit these samples can be obtained via the navigation module $\texttt{Navi}(\cdot)$ in (1), with adaptive velocity

to minimize the total idle time $\tau_{\Xi^+} = (\tau_i + \sum_{j \in \widehat{\mathcal{N}}_i} \tau_j^+)$. As shown in Line 5, it generates the actual schedule of meeting events $\mathbf{c}_i$ and the associated idle time τ_{Ξ^+} as follows:

$$\begin{aligned} &\mathbf{min}_{\mathbf{c}_i'} \quad \tau_{\Xi^+} \\ \textbf{s.t.} \quad &\tau_i^- = \mathtt{A}^\star(\{p_j\}),\, \tau_i^+ = t_j - \xi_j^-(p_j); \qquad (13a) \\ &\tau_j^+ = t_j - t_j^{\mathrm{e}-},\, \forall j \in \widehat{\mathcal{N}}_i,\, p_j \in \widehat{\Omega}_j, \qquad (13b) \end{aligned}$$

where $t_j^{\mathrm{e}-}$ is the end timestamp of executing local plan ξ_j^- for inspector j; $\xi_j^-(t_j)$ returns location of inspector j at time t_j, while $\xi_j^-(p_j)$ outputs the timestamp for inspector j at location p_j. Furthermore, constraint (13a) calculates the travel idle time of the explorer i using $A^\star$ algorithm and the waiting time of the inspector j; (13b) quantifies the waiting idle time of the explorer i. Since non-analytic constraint (13a) cannot be directly applied in the traditional optimization tools, thus a genetic algorithm is leveraged by following the standard steps: the potential sequence $\mathbf{c}_i'$ is jointly encoded as a chromosome; the fitness function is defined as the reciprocal of total idle time, i.e., Fitness $= 1/\tau_{\Xi^+}$; the constraints (13) are enforced by the genetic algorithm; and the standard genetic algorithm procedure [44] is followed to obtain the actual meeting sequence $\mathbf{c}_i$. Finally, the total idle time τ_{Ξ^+} is returned by `OptMeet` algorithm as Line 5. (III) Allocation of Features. Given the confirmed meeting events, the stored new features $\mathcal{F}^+$ are then assigned to the inspectors and appended to the end of their local plans. To determine the optimal assignment and minimize idle time τ_{Ξ^-}, a MVRP is formulated and solved to obtain $\boldsymbol{\varphi}_i$, by setting the end of local plans as initial positions and all features in $\mathcal{F}^+$ as positions to visit. Once $\boldsymbol{\varphi}_i$ is obtained, the next local plans $\{\xi_j^+\}$ are updated by interpolating the shortest path between assigned features, along with the total idle time τ_j^-. Lastly, the total idle time τ_Ξ is derived by adding τ_{Ξ^-} and τ_{Ξ^+} (Line 7). If it is less than the current optimal idle time $\tau_{\Xi^\star}$, the optimal subgroup solution $\Xi_i^\star$ is updated by this solution (Line 9-10). It is important to clarify that our framework does not require the intra-group sharing of global coordinates due to the relative localization within the same group. Particularly, when entering a BBox, all group members adopt the entry point as their local origin. The explorers map the detected features (structural elements, inspection targets) relative to this origin. Finally, the inspectors navigate directly via these relative coordinates without the external alignment between different groups.

3) Algorithm Summary: It is worth noting that the number of subsets $\widehat{\mathcal{N}}_i$ is combinatorial to the size of $\mathcal{N}_\circ^i$, i.e., $\mathcal{O}(2^{|\mathcal{N}_\circ^i|})$. To generate all potential meeting sequences $\widehat{\mathbf{c}}$ has a factorial complexity of $\mathcal{O}(|\widehat{\mathcal{N}}_i|!)$. Then, to determine the optimal sequence of meeting events $\mathbf{c}_i$, the genetic algorithm has a complexity of $\mathcal{O}(|\widehat{\mathcal{N}}_i|^3)$. Finally, the MVRP algorithm to allocate features has a complexity of $O(|\widehat{\mathcal{N}}_i|^{|\mathcal{F}^+|})$.

Lemma 2. *Under the proposed Alg. 2 for the layer of SubGroups, all features $\mathcal{F}$ can be inspected, and the results $\mathcal{S}$ are collected by the explorers in finite time.*

Proof. During each communication event, the explorer assigns the newly discovered features $\mathcal{F}^+$ to the selected inspectors $\widehat{\mathcal{N}}_i$ via the MVRP algorithm in Line 6, which ensures that each inspector is allocated a subset of features $\widehat{\mathcal{F}}_j$. Since the number of features $\mathcal{F}$ is finite, the recursive allocation of features guarantees all features are eventually assigned to inspectors. On the other hand, the proactive communication protocol guarantees that explorers actively communicate with each inspector more than once to minimize the idle time due to waiting. In addition, the inspectors transmit their inspection results $\mathcal{S}$ to the explorer. Since the number of inspectors $\mathcal{N}_\circ$ and communication events are finite, the total time needed to collect all inspection results $\mathcal{S}$ is also finite. ■

Algorithm 2: Simultaneous Optimized Exploration and Inspection `SOEI`$(\cdot)$

Input: $\mathcal{F}_i^+$, $\mathcal{N}_\circ^i$, $\{\xi_j^-\}$.
Output: $\Xi_i^\star$.

1 $\Xi_i^\star \leftarrow$ None, $\tau_{\Xi^\star} \leftarrow \infty$;
2 **foreach** $\widehat{\mathcal{N}}_i \subset \mathcal{N}_\circ^i$ **do**
3 $\widehat{\mathbf{c}}' = \mathtt{SampleLOS}(\{\xi_j^-\})$;
4 **foreach** $\mathbf{c}_i' \in \widehat{\mathbf{c}}$ **do**
5 $(\mathbf{c}_i, \tau_{\Xi^+}) \leftarrow \mathtt{OptMeet}(\mathbf{c}_i', \{\xi_j^-\})$ by (13) ;
6 $(\boldsymbol{\varphi}_i, \boldsymbol{\xi}_i, \tau_{\Xi^-}) \leftarrow \mathtt{MVRP}(\mathbf{c}_i, \mathcal{F}^+, \{\xi_j^-\})$;
7 $\tau_\Xi \leftarrow \tau_{\Xi^-} + \tau_{\Xi^+}$;
8 **if** $\tau_\Xi < \tau_{\Xi^\star}$ **then**
9 $\tau_{\Xi^\star} \leftarrow \tau_\Xi$;
10 $\Xi_i^\star \leftarrow (\widehat{\mathcal{N}}_i, \mathbf{c}_i, \boldsymbol{\varphi}_i, \boldsymbol{\xi}_i)$;
11 **return** $\Xi_i^\star$;

D. Online Execution and Adaptation

1) Rolling Assignment of Exploration Tasks: Since the GCS is fully aware of the location of all BBoxes $\mathcal{B}$, and it coordinates with the explorers directly in the layer of GCS-SubGroups, it is reasonable for GCS to assign these BBoxes to robotic fleets. Moreover, instead of assigning all BBoxes at once, a rolling assignment strategy is adopted in a receding horizon way, which is particularly useful as the actual structure of BBoxes in $\mathcal{B}$ is unknown, making it difficult to predict the exploration time of each BBox. In the initial phase, GCS assigns each explorer $i \in \mathcal{N}_\mathrm{e}$ to the nearest BBox $B_i \in \mathcal{B}$. Then, a subgroup is formed by allocating a specific number of inspectors to each explorer, denoted by $\mathcal{N}_\circ^i \subset \mathcal{N}_\circ$, according to the volume V_{B_i} of the BBox B_i, i.e.,

$$|\mathcal{N}_\circ^i| = \left\lfloor |\mathcal{N}_\circ| \frac{V_{B_i}}{\sum_i V_{B_i}} \right\rfloor, \qquad (14)$$

where $|\mathcal{N}_\circ|$ is the total number of inspectors; and $\lfloor \cdot \rfloor$ represents the floor function. During online execution, when GCS and explorer meet at the designated location p_m^c, each explorer reports the current exploration status of B_i to GCS. Once B_i is fully explored and all inspected features are fed back, the GCS assigns the next nearest BBox to the entire subgroup for execution, until all BBoxes are assigned, as shown in Fig. 8.

2) Handling Mismatch of Meeting Time: Due to motion uncertainty and tracking errors, it is possible that actual arrival time at the designated meeting location is different from the

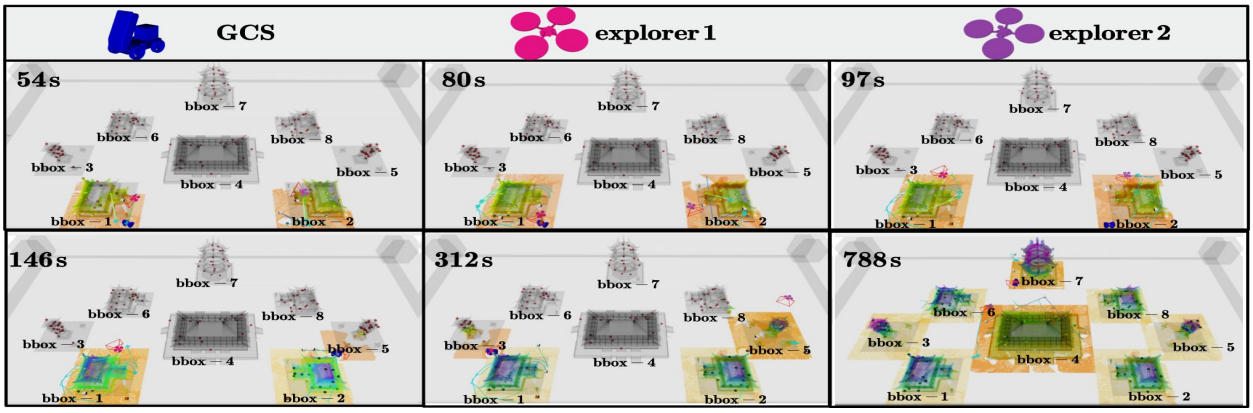

Figure 8: Snapshots of the GCS-to-SubGroup layer in Scenario-A with 1 GCS, 2 explorers and 4 inspectors. At $t = 146s$, BBox-5 is reassigned to explorer 2, and BBox-3 to explorer 1 at $t = 312s$.

planned meeting time, especially in unknown or complex environment. This is called the mismatch of meeting time. To address this challenge, a series of mechanisms are proposed: (I) If the waiting time of GCS for an explorer exceeds a given tolerance $\overline{\delta} > 0$, i.e., $\tau_0 \geqslant \overline{\delta}$, then GCS assumes that this explorer fails and proceeds to communicate with the next explorer. Conversely, if the waiting time of an explorer for the GCS exceeds $\overline{\delta}$, i.e., $\tau_i^+ \geqslant \overline{\delta}$, the explorer has to wait until the GCS arrives; (II) Within a subgroup, if the waiting time of an explorer for an inspector exceeds $\overline{\delta}$, the explorer would continue its local plan. Since the explorer has full knowledge of the local plans of all inspectors, the next scheduled meeting event is appended to the end of the local plan of this inspector. If this tolerance is exceeded again in the next meeting, the explorer would assume that this inspector has failed, in which case the failure recovery mechanism is discussed in the sequel. Last but not least, whenever scheduling conflicts may arise that the explorer should meet with both the GCS and inspectors in close time, higher priority is given to the GCS. This prioritization is justified since GCS-explorer communication occurs infrequently, whereas explorer-inspector communications happen more regularly, allowing remaining data to be deferred to subsequent meetings.

3) Local Adaptation during Exploration: During 3D online exploration, although the optimal path $\widehat{\xi}_i^\star$ of each explorer $i \in \mathcal{N}_\mathrm{e}$ is synthesized given the existing frontiers via Alg. 1, new frontiers may be generated during the exploration process, yielding the need for local adaptation. Thus, to address this issue, Alg. 1 can be triggered in a receding horizon manner by adding new frontiers to the existing set and replanning the path. This iterative re-planning process continues until the explorer reaches the confirmed meeting location p_m^c within t_m^c.

Theorem 1. *The proposed SLEI3D framework ensures that all inspected features $\mathcal{S}$ are collected by the GCS in a finite time, while minimizing the total idle time in* (8)*.*

Proof. Lemma 1 guarantees all features $\mathcal{F}$ are fitted by explorers in finite time, while Lemma 2 ensures all features $\mathcal{F}$ are allocated, inspected and transmitted to explorers by inspectors within finite time. Under the protocol of intermittent communication, the GCS solves the TSP-TW problem to arrive at the meeting location p_m^c at the scheduled time t_m^c, where the explorers transmit the inspected features $\mathcal{S}$. Since both the number of features $\mathcal{F}$ and communication rounds are finite, the GCS collects all inspection results $\mathcal{S}$ within finite time. Furthermore, the strategy of online adaptation can effectively mitigate delays and failures caused by uncertainties. Therefore, the SLEI3D framework guarantees that all features $\mathcal{F}$ are collected back by GCS in a finite time. On the other hand, as re-formulated in Problem 1 algorithms of GCS-to-SubGroups layer coordinate the meeting events between GCS and explorers, to minimize the waiting time. As formulated in Problem 3, algorithm $\texttt{SOEI}(\cdot)$ coordinates the explorer and inspectors in each subgroup, to minimize the idle time. Thus, given the set of currently-known features, the overall plan of the robotic fleet and the GCS minimizes the total idle time in (8) and maximizes the efficiency to collect explored and inspected features. This completes the proof. ■

E. Generalization

1) Robot Failures and Recovery: Consider the following cases: (I) Failure of an explorer: Assume that explorer i fails at $t_\mathrm{f} > 0$, the GCS would wait for the explorer i at the predefined time t_m^c and location p_m^c for a maximum waiting time $\overline{\delta}$. Then GCS determines that explorer i has failed and directly moves to next explorer in its local plan. Subsequently, the meeting events of next rounds are scheduled without considering the failed explorer. In addition, once another subgroup has finished exploring its assigned BBox, it will be reassigned to the BBox of the failed explorer to restart the task of exploration and inspection, along with the remaining inspectors in $\mathcal{N}_\mathrm{o}^i$. (II) Failure of an inspector: Assume that inspector $j \in \mathcal{N}_\mathrm{o}^i$ has failed at $t_\mathrm{f} > 0$, explorer i within the same subgroup would detect its failure after waiting for a maximum duration $\overline{\delta}$. Then, explorer i would exclude inspector j from the subgroup by updating $\mathcal{N}_\mathrm{o}^i \leftarrow \mathcal{N}_\mathrm{o}^i \backslash \{j\}$, after which Alg. 2 is applied to reassign the remaining inspectors.

Beyond the above measures, communication instability between robots (GCS-explorer or explorer-inspector) can be addressed via redundancy. While the baseline mechanism identifies failures after prolonged period of disconnections over $\overline{\delta}$, this might overreact to transient disruptions. Thus, a recovery mechanism at the hardware level is proposed, i.e., each robot carries an ad-hoc mesh network that can be

activated during communication disruption. This network can immediately relay critical status updates while maintaining local coordination. This integrated approach ensures resilience against both permanent failures of robots and temporary degradation of the communication network.

2) Multiple GCS: Multiple GCS units are available, such as in large-scale scenes. In this case, the GCS is assumed to have similar capabilities and all-time connectivity with each other, e.g., regarding the progress of exploration and inspected features. Regarding the communication with explorers, since a subset of explorers is pre-assigned to communicate with a specific GCS, the intermittent communication protocol in Sec. IV-B should be modified by replacing the single TSP-TW with the multiple parallel TSP-TW formulations, to generate a local plan of navigation and communication for each GCS, thus improving overall efficiency.

3) High-priority Features: If the features have different priorities, e.g., some features may require immediate response, the feature allocation module in Alg. 2 can be modified by adding precedence constraints to the inspection tasks associated with high-priority features. Namely, algorithms similar to the MVRP with priority or precedence constraints (MVRP-PC) should be employed. Thus, high-priority features can be inspected first while minimizing the total idle time.

4) Spontaneous Meeting: During execution, the GCS, explorers or inspectors, might meet at locations other than the confirmed meeting locations, which are called spontaneous meetings. In this case, they exchange their local data, without coordinating the next meeting event nor modifying their local plans, such that all confirmed meetings remain valid.

5) Fully-unknown Environment: When the prior information regarding BBoxes is unavailable, an adaptive partitioning method for BBoxes is proposed to dynamically allocate the unexplored regions in $\mathcal{W}$ based on the real-time progress of collaborative exploration. It should be noted that the method relies on prior information about the environmental shape and size, where oddly-shaped workspaces are first enclosed by a regular bounding box before partitioning. As shown in Fig. 4 (b), the whole space $\mathcal{W}$ is initially divided into $|\mathcal{N}_{\mathrm{e}}|$ cubic subspaces with equal volume denoted by $\{B_j\}$. Then, each subgroup autonomously explores its assigned B_j via the framework proposed above, the completion of which is notified to the GCS. The GCS keeps track of the set of unexplored frontiers through $\Psi \triangleq \mathcal{W} \backslash \bigcup_{j \in \mathcal{I}_{\mathtt{comp}}} B_j$, where $\mathcal{I}_{\mathtt{comp}}$ is the set of explored regions. This set Ψ is dynamically partitioned into new set of BBoxes via iterative octree partitioning that preserves the alignment of all axes. This iteration terminates when $\Psi = \varnothing$ or $\min(\dim(B_j)) \leqslant 10.0$m. Subsequent inspections follow the procedure described in Alg. 2, which ensures a complete coverage through hierarchical decomposition.

6) Energy-constrained Fleet Management: When the robots have limited energy capacity and require charging, our framework can be adopted by applying modifications across all layers. To begin with, the robot models should incorporate these constraints. Namely, each robot $i \in \mathcal{N}$ has a limited energy capacity $E_i(t) \leqslant \overline{E} \in \mathbb{R}^+$, which evolves by $\dot{E}_i(t) = -\alpha_i$ with $\alpha_i > 0$ during operation, and $\dot{E}_i(t) = \beta_i$ with $\beta_i > 0$ when charging at the designated station $P_{\mathtt{chg}} \subset \mathcal{W}$. The charging process is triggered when $E_i(t) \leqslant \underline{E} \in \mathbb{R}^+$ and the robot is at the charging station, with a duration $t_{\mathrm{b}} = (\overline{E} - \underline{E})/\beta_i$ for a full charge. This constraint is formally stated as: $0 < E_i(t) \leqslant \overline{E},\ \forall t \in [0,\, T],\ \forall i \in \mathcal{N}$.

To address the above constraint, the proposed framework is adapted with the following three key modifications: (I) The prediction of completion time for an assigned BBox as presented in Sec. IV-B2 must account for the duration of recharging. Consequently, the planned communication time $\widetilde{t}^{\mathrm{c}}_{m+1}$ between the GCS and an explorer is modified as follows:

$$\widetilde{t}^{\mathrm{c}}_{m+1} = t^{\mathrm{c}}_{m+1} + \left\lceil \frac{t^{\mathrm{c}}_{m+1} - t^{\mathrm{c}}_{m}}{\overline{E} - \underline{E}} \right\rceil \cdot (t_b + T_{\mathtt{chg}}), \tag{15}$$

where $\lceil \cdot \rceil$ calculates the minimum recharge cycles, $T_{\mathtt{chg}}$ is the round-trip travel time from one of the four corner points to the charging station $P_{\mathtt{chg}}$ and t_b is the maximum charging duration; (II) During the coordination of GCS-to-SubGroups as described in Sec. IV-B4, the planned meeting time t^{c}_m between the GCS and explorers should also be modified under the following cases: (i) when the remaining energy $(E_0 - \underline{E})/\alpha \geqslant \Delta t_m$, where $\Delta t_m = t^{\mathrm{c}}_m - t^{\mathrm{c}}_{m-1}$ denotes the time interval between two consecutive meetings, the planned t^{c}_m remains feasible under the energy constraint. (ii) if $(E_0 - \underline{E})/\alpha < \Delta t_m$, the GCS needs an intermediate charging, for which the meeting time is adjusted by:

$$\tilde{t}^{\mathrm{c}}_m = t^{\mathrm{c}}_m + \left\lceil \frac{\Delta t_m - E_0}{\overline{E} - \underline{E}} \right\rceil \cdot (T^0_{\mathtt{chg}} + t_b),$$

where $T^0_{\mathtt{chg}}$ denotes the round-trip travel time between the meeting point p^{c}_m and the charging station; (III) During the coordination within each SubGroup, the initial assignment ϕ_i computed via solving the MVRP as described in Sec. IV-C2 can be reformulated to generate an energy-unconstrained routing sequence $\mathcal{F}^+$ for each inspector, i.e., by predicting the energy consumption along the local plan of each inspector and inserting charging events as needed. The planned timestamps for subsequent inspection events are shifted accordingly.

V. Numerical Experiments

To further validate the effectiveness of the proposed method, extensive numerical experiments for large-scale systems are conducted, of which the performance is compared against several state-of-the-art methods. The proposed method is implemented in `Python3` within the framework of `ROS`, and tested on a workstation with Intel(R) i9-13900KF 24-Core CPU @3.0GHZ with a RTX-4090 GPU. Simulation videos can be found in the supplementary material.

A. System Description

The simulated robotic fleet consists of UAVs as explorers and inspectors, and UGVs as the GCS, which is deployed in a light-weight simulator [45], [46]. As shown in Fig. 9, the following **four** scenarios are considered. Scenario-A: 1 GCS, 2 explorers and 4 inspectors are deployed in a cluster of ancient structures of size $60 \times 50 \times 9m^3$ to validate the performance of the GCS-to-SubGroups layer as described in Sec. V-B1; Scenario-B: 1 explorer and 3 inspectors are deployed in a large

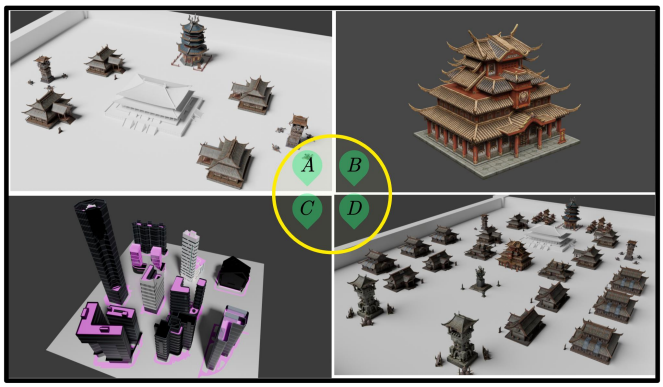

Figure 9: Scenarios tested in the numerical experiments: Scenario-A with a set of small ancient structures; Scenario-B with a single ancient structure; Scenario-C with a medium-scale city structures; and Scenario-D with a large-scale ancient site.

and single architecture structure of size $18 \times 20 \times 15m^3$ to validate the performance of the SubGroups layer as described in Sec. V-B2; Scenario-C: 1 GCS, 4 explorers and 8 inspectors are deployed in a medium-scale city of size $70 \times 60 \times 30m^3$, to validate the performance of the overall scheme as described in Sec. V-B3; and Scenario-D: 1 GCS, 8 explorers and 40 inspectors are deployed in a large-scale ancient site of size $120 \times 160 \times 20m^3$ to validate the overall performance.

To bridge the gap between theoretical validation and practical deployment in high-fidelity simulations, our experimental framework is constructed with three meticulously designed core modules: perception, planning, and communication. The system implementation leverages a novel lightweight architecture that diverges from conventional Gazebo-based workflows through: (I) Perceptual realism via sensor emulation: Laser rangefinders and RGB-D cameras are simulated with configurable noise models (±2cm ranging error, 5% depth distortion), replicating Gazebo plugin functionalities while eliminating computational overhead. (II) Environment abstraction: Operational spaces are discretized into point cloud representations (0.1m resolution voxels) through RVIZ integration, preserving geometric fidelity while enabling real-time collision checking. (III) ROS-native interoperability: Standardized message interfaces ensure seamless transition between simulated and physical platforms. The system implementation details are specified as follows: A 3D Euclidean Signed Distance Field (ESDF) map is generated via [47] as local map, with a 5 m-range depth camera and odometry sensor as a volumetric map of the environment. Then, the Area of Interest (AoI) identification pipeline concurrently processes the synchronized data streams at 0.5 Hz: RGB images analyzed by predicting the depth and semantic information via MiDas network and DeepLabV3+ for 3D reconstruction of geometric features, and object recognition by YOLOv7. Each explorer and inspector navigates using a kinodynamic motion planner to generate collision-free path, which contains multiple topologically distinct waypoints capturing the structural complexity of the 3D environment, with a maximum speed of $2m/s$ and acceleration of $2m/s^2$. Feature fitting, detection and inspection are facilitated by inspectors equipped with a field-of-view (FOV) camera, which has a left and right view of 90°, a front view of 60°, and a detection range of 5 m. Once features are within the FOV, the features can be fitted via $\texttt{Fit}(\cdot)$ in (4) or inspected via $\texttt{Inspect}(\cdot)$ in (5) automatically by the explorers or inspectors. Moreover, the communication within the robotic fleet is restricted to a range of $5m$ and has a LOS.

B. Results

The results associated with the four scenarios are summarized below, including generalization to robot failures, multiple GCSs and high-priority features. Lastly, scalability and robustness analyses are performed w.r.t. fleet size, various uncertainties and different duration of inspection tasks.

1) Evaluation of the Layer of GCS-to-SubGroups: As depicted in Fig. 8, the scenario-A includes 1 GCS, 2 explorers and 4 inspectors, to explore an area of 8 BBoxes. To initiate the exploration process, the GCS assigns two inspectors to each explorer as subgroups based on the fleet size and number of BBoxes, using the rolling assignment strategy. Then, these subgroups are assigned to the nearest BBoxes with an average assignment time of $1ms$. Subsequently, each explorer is guided by Alg. 1 with an average planning time of $26ms$, which dynamically adapts the exploration path based on the current position, velocity and the confirmed meeting events $\mathcal{C}$. At the same time, the communication coordination algorithm has an average computation time of $3.5ms$, which determines the optimal visit sequence between the GCS and the explorers. For instance, during the first meeting, the GCS is set to visit BBox-1 to meet explorer 2, then proceed to BBox-2 for explorer 1, return to BBox-1 for another interaction with explorer 2, and finally head to BBox-5 for explorer 1 again, as shown in Fig. 8. The prediction algorithm of the task completion time in (9) takes on average $0.47ms$, with an average prediction error around $13.2s$. The execution process can be further explained in the following timeline. At $t = 54s$, the GCS follows the confirmed meeting event with explorer 2, and arrives early at the meeting location of BBox-1, as shown in Fig. 11. At $t = 80s$, explorer 2 reaches the specified location to meet with GCS. Similarly, the GCS waits for explorer 1 at $t = 97s$ at the meeting location of BBox-2 earlier than the scheduled time. At $t = 146s$, explorer 1 meets with the GCS and a new task to explore BBox-5 is assigned to it. After meeting with GCS at $t = 312s$, explorer 1 sends the inspected features, and GCS assigns the nearest BBox-3 as the new task to explorer 1. After $t = 788s$, all 150 features are collected by the GCS.

Moreover, as illustrated in Fig. 11, the number of meetings for each BBox is less than 3, i.e., the proposed algorithm can accurately predict the completion time of each exploration task. Moreover, it is worth noting that the actual arrival times of all explorers for the meeting events are consistently earlier than the planned meeting time, indicating that Alg. 1 can ensure the timely arrival within the specified time window, thus reducing the idle time for the GCS and the explorers.

2) Evaluation of the Layer of SubGroups: This section highlights the intra-group dynamics in Scenario-A, as depicted in Fig. 9, and the influence of different inspection time t_q.

(I) **Overall execution**. As illustrated in Fig. 10, the robot motion and actions within the subgroup are monitored during

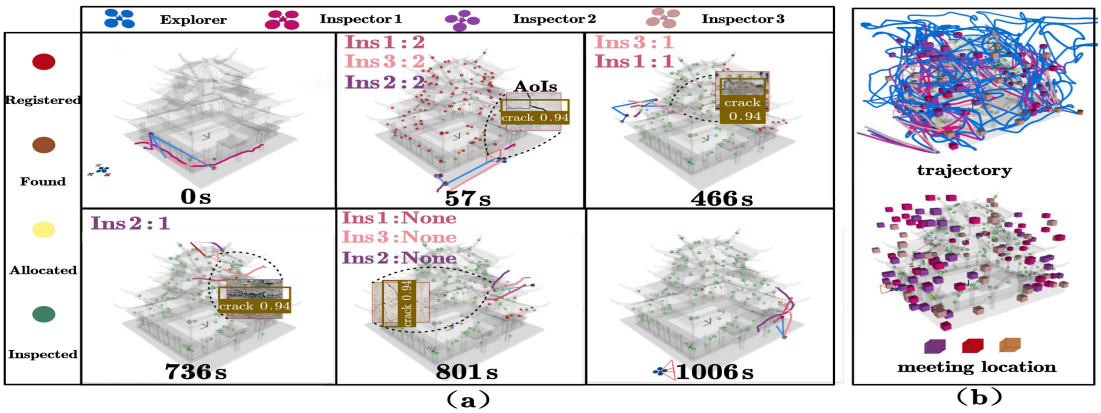

Figure 10: Evolution of the layer of SubGroups in Scenario-B consisting of one explorer and three inspectors: (**a**) snapshots of the planned trajectories of the explorer and inspectors at different time instants; (**b**) the entire trajectories and the complete meeting events of all robots.

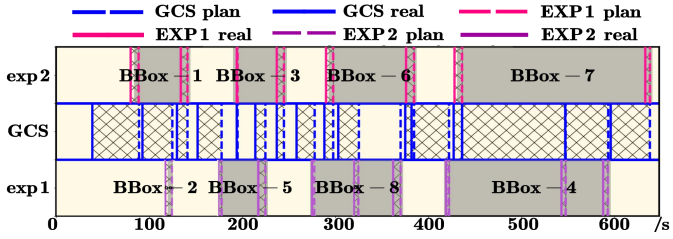

Figure 11: The planned and actual meeting events between the GCS and two explorers in Scenario-A. The planned meeting time for the GCS (blue dashed lines) aligns with the explorers (pink and purple dashed lines), indicating the confirmed meeting event and the target BBox. The solid lines represent the actual arrival time, which are bound with the planned time of the same meeting by latticed areas.

the execution in Scenario-B, along with the exploration and fitting of features. The Alg. 2 is triggered every $5s$ if new features $\mathcal{F}^+$ are discovered to optimize the subgroup solutions Ξ_i with an average computation time of $1.384s$. Specifically, given the executing local plans $\{\xi_j^-\}$ of all inspectors, the explorer utilizes the $\texttt{SmapleLos}(\cdot)$ function which has an average runtime of $1.3s$, while the $\texttt{OptMeet}(\cdot)$ has an average runtime of $0.04ms$ to optimize the inspectors $\widehat{\mathcal{N}}_i$ and the meeting events $\mathbf{c}_i$. Subsequently, the explorer assigns the newly-fitted features to the selected inspectors by invoking the modified $\texttt{MVRP}(\cdot)$ algorithm with an average runtime of $0.08s$. Lastly, the local plans $\{\xi_j^+\}$ of the inspectors are updated based on the executing local plans $\{\xi_j^-\}$ and assigned features $\boldsymbol{\varphi}_i$, by invoking the $\texttt{Navi}(\cdot)$ with an average computation time of $0.05s$. During the communication phase, the explorer transmits the allocated features $\boldsymbol{\varphi}_i$ and the updated local plans $\{\xi_j^+\}$ to the respective inspectors, ensuring the consistency of tasks across the subgroup. Some representative moments are described as follows: At $t = 57s$, the explorer decides to meet with the inspector 1 which is assigned 2 features, then with the inspector 3 which is assigned 2 features, and finally the inspector 2 which is assigned 2 features. At $t = 466s$, the explorer meets with the inspector 3 first which is assigned 1 feature, followed by the inspector 1 and assigned 1 feature. The explorer avoids meeting with inspector 2 due to longer travel distance, thereby reducing the total idle time. At $t = 736s$, the explorer chooses to meet only inspector 2, which is assigned the newly discovered features. These features are in the proximity of inspector 2 and there are no remaining features to inspect. At $t = 801s$, the explorer meets with no inspectors, as all inspectors have ongoing inspection tasks and are far away. Moreover, the entire trajectories of all robots within the subgroup and the meeting locations of the subgroup are also shown. It can be seen that the trajectory of the explorer is rather complex due to the online adaptation to meeting events with all inspectors, whereas the trajectories of the inspectors are smoother as the features are appended to their local plans incrementally.

Last but not least, the online change of the status of each robot is shown in Fig. 12, e.g., "explore", "travel", "inspect" and "wait"; the evolution of the number of "registered", "found", "allocated", and "inspected" features; and the communication events between the explorer and inspectors. It can be seen that the explorer spends 60.35% of the time to explore and fit AoIs across the entire scenario. The inspectors primarily travel to features for inspection with an average waiting time of $33s$. In addition, the middle figure shows that the explorer meets with all, some or none of the inspectors at different moments, with the average communication cycle of $6.8s$. The bottom sub-figure shows that 150 features are fully inspected within $1006s$, yielding a 100% coverage.

(II) **Different Inspection Time**. To evaluate the effect of different inspection times t_q on the performance of our proposed method, we have conducted a series of experiments with different t_q, ranging from $1s$ to $10s$. The metric to compare includes the average number of features assigned per meeting. The results show that the number of assigned features monotonically decreases from 3.11 to 1.65 as t_q increases from $1s$ to $8s$. Thus, more frequent meetings are required if it takes shorter duration to inspect the features.

3) Full-process Simulation: To validate the complete performance as shown in Fig. 13, large-scale simulations are conducted under different sizes of workspace and robotic fleets: Scenario-C with 1 GCS, 4 explorers and 8 inspectors, and Scenario-D with 1 GCS, 8 explorers and 40 inspectors. As described earlier, the two layers are integrated with different frequencies. In Scenario-C, the average meeting cycle is $40.6s$ between GCS and explorers, and the average meeting cycle is $6.8s$ between explorers and inspectors. In contrast to Scenario-D, these rates are $63.2s$ and $5.5s$, respectively. The

This article has been accepted for publication in IEEE Transactions on Automation Science and Engineering. This is the author's version which has not been fully edited and content may change prior to final publication. Citation information: DOI 10.1109/TASE.2025.3643166

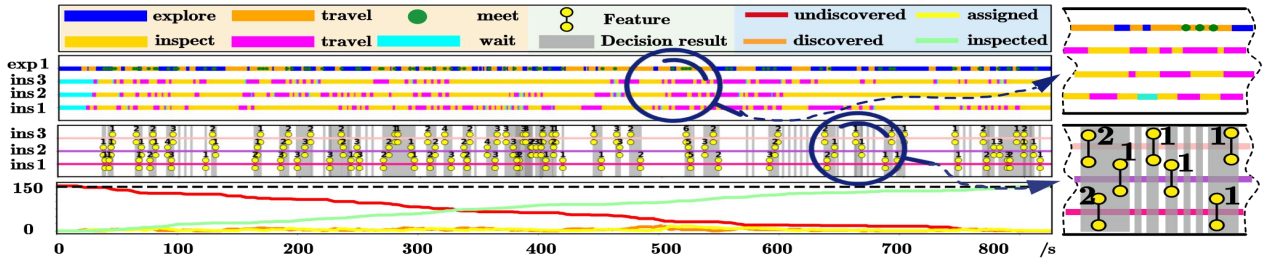

Figure 12: Top: Evolution of the status of all robots within the subgroup in Scenario-B: explorers with exploring (deep blue), traveling (deep orange) and meeting (green); inspectors with inspecting (light orange), traveling (pink) and waiting (cyan). **Middle**: Planning results of explorers during the meetings with inspectors, represented by gray boxes. Hammer-shaped symbols with different inspectors along the timeline indicate the sequence of planned meeting events, with the number of features assigned to each inspector. **Bottom**: Progression of different status associated with the features over time: undiscovered (red), discovered by explorers (orange), assigned to inspectors (yellow), and inspected by inspectors (green).

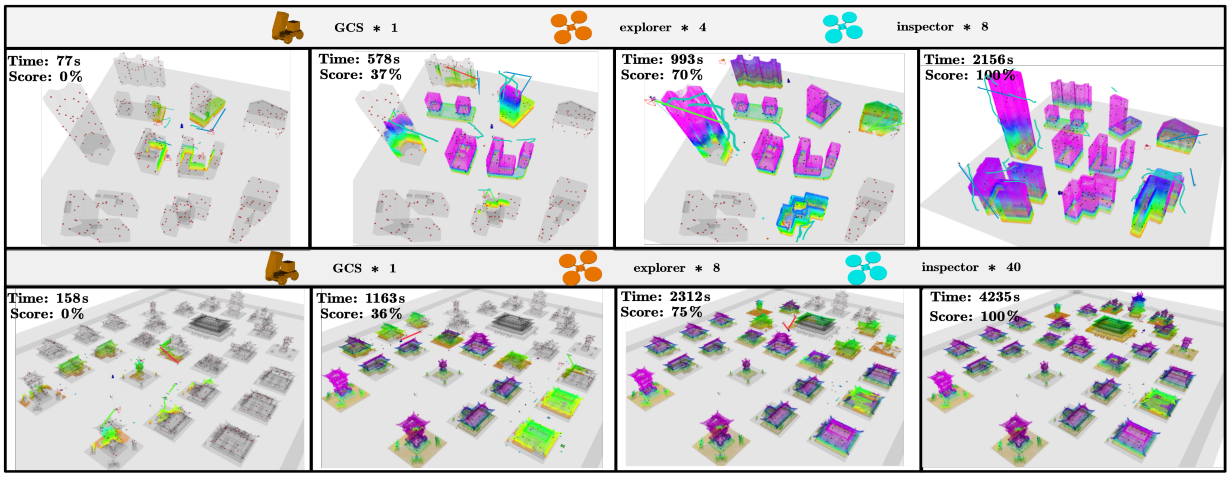

Figure 13: Snapshots of overall execution for Scenario-C under 1 GCS, 4 explorers and 8 inspectors (**Top**); and Scenario-D under 1 GCS, 8 explorers and 40 inspectors (**Bottom**).

rolling assignment strategy further improves the efficiency of different subgroups by dynamically reallocating BBoxes. In Scenario-C, the explorers complete tasks at $578s$ and $993s$, which are then reassigned to nearby BBoxes to minimize idle time. Similarly, in Scenario-D, explorers are reallocated at $1163s$ and $2321s$. On average, each explorer is assigned 2.5 BBoxes in Scenario-C and 3.3 BBoxes in Scenario-D, with an average mission time of $529s$ and $513s$, respectively. This indicates that the proposed method can effectively balance the task allocation for each subgroup across different scenarios. It is worth noting that the explorers achieve a 100% success rate in reaching meeting locations on time in both scenarios, while the GCS occasionally experiences minor delays in Scenario-D due to overlapping tasks in cluttered environments. Moreover, the average number of communications between the GCS and each subgroup is less than 3 in both scenarios, indicating that the proposed algorithm is effective in predicting the completion time. The layer of SubGroups also demonstrates adaptability in complex environments, such as cluttered buildings in Scenario-C and intricate structures in Scenario-D. In both cases, the proposed method achieves 100% feature coverage for $1006s$ in Scenario-C and $2006s$ in Scenario-D.

The overall efficiency is influenced by multiple factors, with the exploration efficiency of the explorers being particularly critical for enhancing the feature discovery and the inspection process. A key metric quantifying exploration efficiency is the overlap rate, which reflects redundant coverage across robots. In our framework, the inter-group exploration overlap is fully eliminated via the pre-assigned bounding boxes (BBoxes) for the dedicated explorers in the robotic fleet. However, intra-group operations by single explorer rather than multi-explorer exploration exhibit an average 15% overlap rate across the four scenarios, i.e., $20\%, 10\%, 13\%$, and 17% in Scenario A–D respectively. This result aligns with the overlap rate for single-robot exploration in [48]. By enforcing a strict zero inter-group overlap rate and suppressing intra-group overlap to minimal levels, the proposed approach enhances exploration efficiency through systematic reduction of redundant exploration.

C. Comparisons

To further validate the effectiveness of the proposed method (as **SLEI3D**), a quantitative comparison is conducted against **six** strong baselines:

(i) **CARIC**, which is based on a hierarchical framework for simultaneous exploration and inspection proposed in [34]. The robots are partitioned into teams, where each team is independently assigned to specific sub-regions, and then relays the inspection results to a static GCS under the LOS communication. For a fair comparison, a modification is added such that the GCS can move to communicate with the explorers.

This article has been accepted for publication in IEEE Transactions on Automation Science and Engineering. This is the author's version which has not been fully edited and content may change prior to final publication. Citation information: DOI 10.1109/TASE.2025.3643166

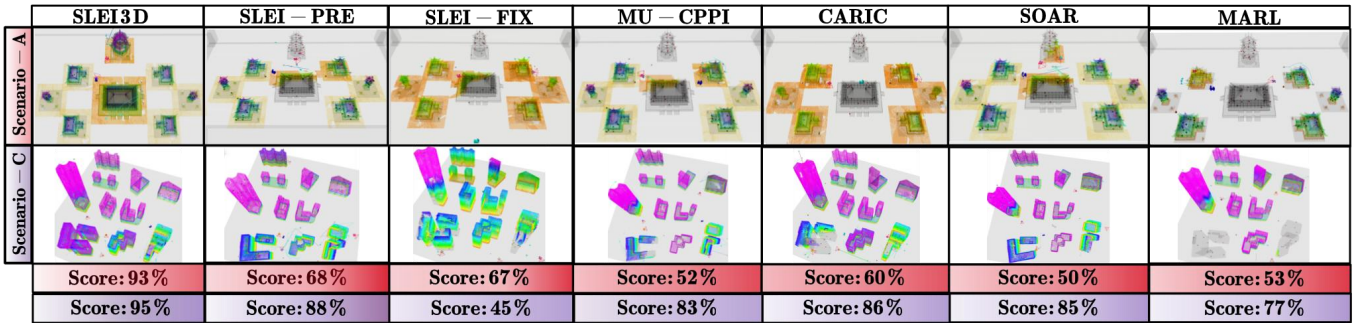

Figure 14: Comparison of the final score between the proposed method (SLEI3D) and six baselines in Scenario-A and Scenario-C.

(ii) **SOAR**, which is built upon the work in [33]. Only one explorer identifies the unknown areas and generates viewpoints that are subsequently assigned to inspectors through global all-to-all communication. However, it cannot handle scenarios involving multiple explorers under limited communication, nor does it account for the need to return information back to the GCS. To ensure a fair comparison with our method, SOAR is only adopted for the task of assigning features from explorers to inspectors, while the rest of components follows the proposed framework to be compatible with the problem settings.

(iii) **MU-CPPI**, which is based on the exploration-then-inspection framework proposed in [32], The robots first explore the entire environment, and then the local plans of inspection are generated based on the exploration results. However, as this approach does not account for a movable GCS, limited communication constraints and simultaneous exploration and inspection. Therefore, above method can be only leveraged for the subgroups layer to guide explorers to meet with the inspectors in the subgroup. The rest of components follow the proposed framework to match the problem settings.

(iv) **MARL**, a multi-robot strategy for collaborative exploration via multi-agent reinforcement learning (MARL) as seen in [25], [49], [50]. These works develop end-to-end coordination strategies that jointly optimize exploration policies and collision-free motion planning. However, they exclusively focus on the exploration phase within our problem formulation, without addressing communication requirements between inter-and-intra groups. Thus, the MARL module is adopted only to replace the exploration strategy for explorers as presented in Sec. IV-B3 while retaining other components of the proposed framework to ensure system compatibility.

(v) **SLEI-PRE**, where all BBoxes are initially allocated to the explorers, i.e., each explorer follows a fixed order to explore the designated BBoxes, instead of relying on dynamic allocation by the GCS.

(vi) **SLEI-FIX**, where the GCS remains stationary at its initial position throughout the entire process. Consequently, the explorers are required to return to the GCS at fixed intervals for communication.

The above methods are evaluated across both scenario-A and scenario-C, each of which 3 tests are conducted. The experimental results are summarized in Fig. 14 and Table I.

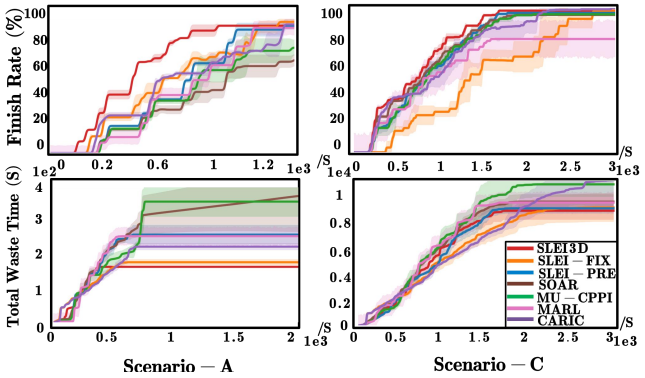

Figure 15: Comparison of the number of collected features over time, between the proposed method and six baselines over three runs.

Collected features by the GCS over time are shown in Fig. 15, where the execution time for scenario-A is $600s$ and $1660s$ for scenario-C. For both scenarios, SLEI3D takes the least amount of time $743.7s$ and $1699s$ to collect all features (thus the highest efficiency) in scenario-A and scenario-C, compared to CARIC ($1009s$ and $2659s$), SOAR ($1110s$ and $1908s$), MU-CPPI ($1239s$ and $2117s$), MARL ($932.5s$ and $1648s$), SLEI-PRE ($988.7s$ and $1767s$), and SLEI-FIX ($939.7s$ and $2462s$).

Furthermore, it is evident that employing a movable GCS facilitates faster task completion and less idle time, compared with SLEI-FIX ($939.7s$ and $2462s$). In addition, while both SLEI3D and SLEI-PRE achieve similar finish rates ((94.0% and 96.7%) vs. (92% and 95.3%)), the dynamic allocation of BBoxes allows for much less idle time, compared with SLEI-PRE. SLEI3D also facilitates more effective collaboration between explorers and inspectors. This is evident by the higher number of meeting events between explorers and inspectors, particularly in scenario-C, where SLEI3D achieves an average of 279.7 meetings, compared to 199.3 for SLEI-PRE and 188.7 for SLEI-FIX. This difference is even more pronounced in comparison to CARIC and SLEI3D. While CARIC adopts a simpler intra-group communication strategy, it lacks the adaptability for complex tasks. SLEI3D achieves faster task completion (($743.7s$ and $1699s$) vs. ($1009s$ and $2659s$)) and less idle time (($1434.5s$ and $7920.3s$) vs. ($1967s$ and $10032s$)). Additionally, MARL trained specifically on scenario-A, exhibits significant performance degradation when transferred to scenario-C. This is evident from the substantial drop in success rate (from 92.4% to 77.8%) between the two scenarios, as shown in Table I. In contrast, our approach demonstrates superior generalization capability with consistent success rates

TABLE I
COMPARISON OF BASELINES ACROSS TWO SCENARIOS.

Scene	Method	Finish Rate (%)				Finish Time (s)				GCS-EXP Meeting (#)				EXP-INS Meeting (#)				Total Waste Time (s)			
		Avg	Std	Max	Min	Avg	Std	Max	Min	Avg	Std	Max	Min	Avg	Std	Max	Min	Avg	Std	Max	Min
Scenario A	CARIC	97.6	2.1	100	96	1009	29.6	1037	978	7.3	0.6	8	7	57.3	1.15	58	56	1967	72.4	2018.3	1884.2
	SLEI-PRE	92	2	94	90	988.7	116.3	1100	868	10.3	0.6	11	10	90	6.1	97	86	2259.4	292.9	2586.2	2020.5
	SOAR	73	1	74	72	1110	141.1	1254	972	10.3	1.5	12	9	174	14.1	189	161	2716.1	603.9	3304.6	2097.8
	MU-CPPI	83.7	2.5	86	81	1239	72.4	1322	1189	9.7	1.5	11	8	83	4.4	86	78	3104.1	467.9	3616.8	2700.1
	SLEI-FIX	96	2.7	98	93	939.7	66.30	1002	870	10	0	10	10	52.7	1.2	54	52	1551.9	85.9	1636.6	1464.8
	MARL	92.4	4.2	97.1	87.5	932.5	120.3	1060	800.3	13.5	4.2	18	9	93.5	13.2	108	88	2218.8	512.9	3000.8	1737.2
	SLEI3D	**94.0**	1	94	93	**743.7**	208.5	976	573	**13.7**	3.5	17	10	**84.7**	11.9	98	75	**1434.5**	17.0	1454.1	1423.6
Scenario C	CARIC	98.7	0.6	99	98	2659	317.5	3007	2385	8.7	0.6	9	8	182.7	11.1	194	172	10032	2178.2	12288	7940.4
	SLEI-PRE	95.3	1.2	96	94	1767	102.9	1882	1684	38.3	1.2	39	37	199.3	6.8	207	194	8085.5	411.1	8459.7	7645.4
	SOAR	94	1	95	93	1908	54.2	1954	1848	43	3	46	40	415.3	11.2	425	403	8542.1	616.3	9229.8	8039.9
	MU-CPPI	94.7	0.6	95	94	2117	51.5	2172	2070	44	10.2	55	35	165.3	29.1	198	142	9725.3	1048.1	10742	8648.6
	SLEI-FIX	96.7	1.2	98	96	2462	365.5	2870	2165	14	0	14	14	188.7	25.5	218	172	8809.4	490.1	9252.3	8282.9
	MARL	77.8	5.5	85	70	1648	210.8	2000	1314	37	0	37	37	162.7	28.6	200	130	8479.1	504.2	9000.1	7800.5
	SLEI3D	**96.7**	1.5	98	95	**1699**	66.7	1776	1658	**42**	3.5	44	38	**279.7**	80.8	353	193	**7920.3**	733.6	8767.4	7496.8

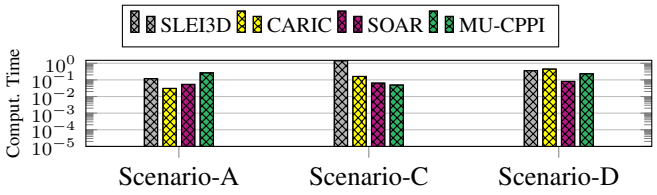

Figure 16: Comparison of computation time between SLEI3D and other methods in different scenarios.

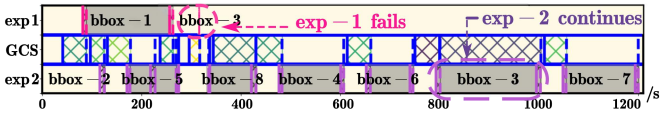

Figure 17: Failure detection and recovery when explorer 1 fails at $t = 338s$ in Scenario-A.

across both scenarios (94.0% vs. 96.7%). This performance disparity highlights the inherent limitations of pure learning-based methods like MARL, which tend to overfit to their training environments. Our hybrid architecture effectively mitigates this issue through its adaptive task allocation mechanism and geometric-aware coordination, enabling robust performance in both familiar and novel scenarios. Furthermore, MARL shows high instability with large success rate deviations (4.2% vs. 5.5%), while SLEI3D demonstrates consistent robustness across runs (1.0% vs. 1.5%). Lastly, SLEI3D achieves the lowest idle time in both scenarios, with $1434.5s$ and $7920.3s$ in scenario-A and scenario-C, respectively, compared to CARIC ($1967s$ and $10032s$), SOAR ($2716.1s$ and $8542.1s$), MU-CPPI ($3104.1s$ and $9725.3s$), MARL ($2218.8s$ and $8479.1s$), SLEI-PRE ($2259.4s$ and $8085.5s$), and SLEI-FIX ($1551.9s$ and $8809.4s$). In summary, SLEI3D effectively addresses the challenges posed by the state-of-the-art frameworks such as CARIC, SOAR and MARL, as well as the SLEI variants.

Furthermore, as Fig. 16 illustrates, the comparative analysis of computation time with baseline methods (CARIC, SOAR and MU-CPPI) reveals SLEI3D exhibits higher average computation times (0.6325 s vs. 0.2128 s vs. 0.0662 s vs. 0.1827 s) across scenarios, primarily due to the $\texttt{SOEI}(\cdot)$ optimization. MU-CPPI achieves the shortest processing times, whereas SLEI3D exhibits stable computation times (0.118–$1.4225s$). Despite higher computational costs, SLEI3D's method yields significant performance improvements as analyzed in Table I.

D. Generalizations

1) Robot Failure: As described in Sec. IV-E, the proposed method can detect and recover from potential robot failures of explorers and inspectors during execution. Particularly, the parameter $\bar{\delta}$ is set to $10s$.

(I) **Explorer Failure**. Consider the same setting as in Sec. V-B1 with 1 GCS, 2 explorers and 4 inspectors in Scenario-A, where one explorer fails online. The final meeting results between GCS and explorers are shown in Fig. 17. Explorer 1 fails at $t = 338s$ *before* the meeting with GCS at BBox-3. This failure is then detected by GCS at the predefined time and location after waiting for $10s$. Then, the GCS directly proceeds to the next meeting event at BBox-8 to communicate with explorer 2. As shown in Fig. 17, the waiting period of GCS results in a slight delay of its arrival at BBox-8 compared to the planned time. Following the proposed failure recovery mechanism, the whole subgroup belonging to explorer 2 is reassigned to BBox-3 to restart the task, as the failed explorer 1 is unable to relay the inspection results of BBox-3 to the GCS. The overall mission is completed at $1215s$, which is slightly longer than the $788s$ in Fig. 8 without failures.

(II) **Inspector Failure**. Consider the same setup as in Sec. V-B2, but two inspectors fail consecutively during execution. The overall changes in robot state, decision-making results, and completion status of features are summarized in Fig. 18. Inspector 2 fails at $t = 683s$ *before* meeting with the explorer, of which is detected by the explorer after waiting for $10s$ at the end of its local plan. Then, inspector 2 is excluded from the set of active inspectors that are known to the explorer. In addition, it is clear that once the explorer detects the failure of inspector 2, no further features are assigned to inspector 2. After inspector 3 fails at $t = 825s$, the explorer behaves similarly to detect this failure. Lastly, the overall mission is completed at $t = 1380s$, which is higher than the $1006s$ in the nominal scenario without failures. It is worth noting that after the failures of inspectors 2 and 3, the explorer tends to have fewer meetings but assign more features.

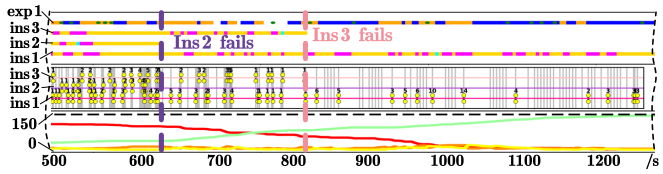

Figure 18: Failure detection and recovery when inspector 2 fails first at $t = 683s$, followed by inspector 3 fails at $t = 825s$ in Scenario-B.

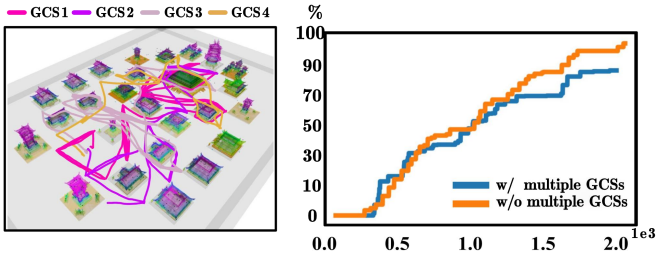

Figure 19: Scenario-D with 4 GCS, 8 explorers and 40 inspectors: final meeting trajectories of all GCSs (**Left**); comparison of collected features over time (**Right**).

2) Multiple GCS: The proposed SLEI3D algorithm is evaluated in Scenario-D under two configurations: one leveraging a multi-GCS setup with 4 GCSs, 8 explorers, and 40 inspectors, and the other employing a single-GCS configuration. Specifically, each GCS is pre-assigned to specific subsets of BBoxes and a subset of explorers, each of which acts independently. The final trajectories of all GCSs and the collected features along with time are shown in Fig. 19. It is evident that each GCS successfully meets with the assigned explorers, thus collecting all features. However, it is interesting to notice that SLEI3D with multiple GCSs initially achieves a faster feature collection compared to its single-GCS counterpart. However, as the process progresses, the SLEI3D catches up and eventually surpasses the performance of the multi-GCS configuration. This is due to the fact that all explorers start from the same location and are assigned BBoxes of similar sizes. In other words, the completion times of these BBoxes are almost synchronized via the proposed routing scheme for multiple GCSs, which allows each GCS to concurrently collect features from its assigned BBoxes. In contrast, SLEI3D can only sequentially collect features from multiple BBoxes, yielding a much slower collection of features. As the mission proceeds, the subsets of BBoxes to be explored varies significantly in volume, yielding a diverse distribution of completion time. Consequently, the benefits of having multiple GCSs diminish as the rate of feature collection becomes less dependent on the distributed coordination. Thus, it shows that the multi-GCS counterpart is particularly suitable for scenarios requiring simultaneous feature collection across a wide distribution of locations.

3) High Priority Features: To further validate SLEI3D with high-priority features, 50 features of the 150 features in Scenario-B are selected as high-priority features. Snapshots of the inspector trajectory along with the priority of these features are shown in Fig. 20, which highlights the fact that high-priority features are inspected first. Namely, the inspector prioritizes 3 high-priority features out of 5 features. Moreover, the collection of high-priority features or all features

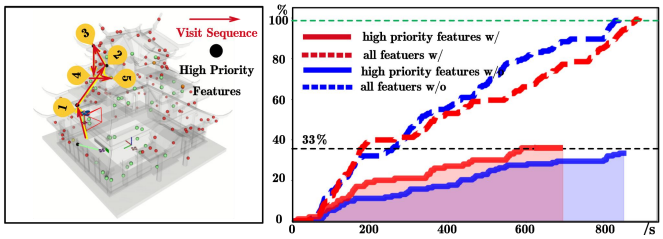

Figure 20: High-priority features in Scenario-B with 150 features and 50 high-priority features: inspection sequence of features with high-priority (**Left**); comparison of collected high-priority features over time (**Right**).

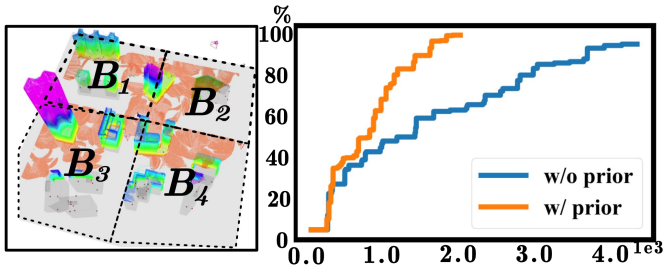

Figure 21: Overall evolution for our system without any priors under Scenario-C (**left**); comparison of collected features over time (**Right**).

over time are also shown. It can be seen that SLEI3D with consideration for high-priority features achieves much faster collection of high-priority features than SLEI3D, while the overall completion time is slightly longer ($842s$ vs. $893s$). This is because prioritizing high-priority features prevents simultaneous optimization of the allocation for all features, resulting in an increase in the overall completion time.

4) Fully-unknown Environment: To validate SLEI3D's capability in completely unknown environments, comparative experiments are conducted for Scenario-C under 1 GCS, 4 explorers, and 8 inspectors with and without prior information regarding BBoxes. As shown in Fig. 21, prior-free exploration exhibits significantly slower feature discovery rates for explorers. This delay is due to the absence of BBoxes, compelling explorers to exhaustively explore uniform subspaces without prioritizing targeted areas. Consequently, the GCS experiences significant delays in collecting the features (1832s vs. 4000s), which validates the effectiveness of the proposed mechanism for adaptive partitioning. It also highlights how prior information regarding BBoxes can accelerate the overall mission of exploration and inspection.

5) Heterogeneous Capability of Explorers: To verify the support for heterogeneous fleets, the explorers in Scenario-C are set to different sensing ranges ($6m$, $8m$, $10m$, $12m$) versus homogeneous units (uniform $5m$ sensors). As shown in Fig. 22, the heterogeneous system achieves faster feature discovery and inspector dispatch through longer ranges. This takes 40% less time to collect around 90% of features ($1005s$ vs. $1656s$), compared to the homogeneous counterparts. Notably, explorers with larger sensing ranges are prioritized for larger BBoxes via receding-horizon allocation by GCS , which aligns with the time-minimization objective as presented in (7). The results confirm the compatibility of the proposed framework to heterogeneous fleets, with the overall performance positively correlating with increased sensor ranges.

This article has been accepted for publication in IEEE Transactions on Automation Science and Engineering. This is the author's version which has not been fully edited and content may change prior to final publication. Citation information: DOI 10.1109/TASE.2025.3643166

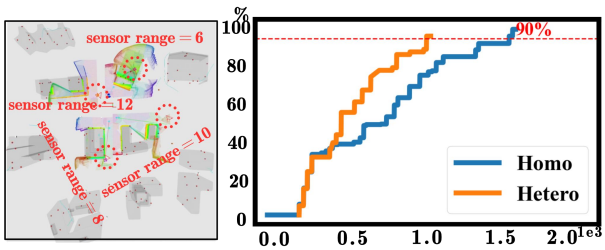

Figure 22: Heterogeneous sensor range of explorers in Scenario-C with 1 GCS, 4 explorers and 8 inspectors (**left**); comparison of collected features over time (**right**).

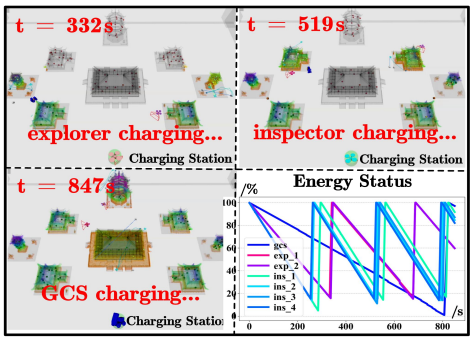

Figure 23: The representative snapshots of recharging for diffrent role of robots via returning to the fixed charging station under Scenario-A and the overall evolution of energy status for entire fleet.

6) Energy-constrained Fleet Management: To validate that the proposed framework can handle energy constraints as described in Sec. IV-E6, a team comprising of 1 GCS with $\overline{E}_0 = 800\ mAh$ energy, 2 explorers ($\overline{E}_i = 400\ mAh, \forall i \in \mathcal{N}_e$), and 4 inspectors ($\overline{E}_j = 300\ mAh, \forall j \in \mathcal{N}_o$) is deployed within the Scenario-A. A unified protocol for recharging is activated when the energy level of any robot drops below $\underline{E} = 20\%\overline{E}$, with all charging stations providing $\beta = 10\%\overline{E}$ charging rate per second. The key events captured in Fig. 23 demonstrate the overall efficiency under energy constraints: At $t = 332$ s, Explorer 1 initiates the protocol of recharging once it reaches the critical threshold $\underline{E}$ (as visualized in the plot of energy status), followed by a similar event for Inspector 3 at $t = 540$ s. The GCS executes its scheduled recharge at $t = 780$ s while maintaining the planned communication events with the explorers. During 878 s when all AoIs are inspected, the team performs in total 1, 2 and 3 recharging events for the GCS, explorers and inspectors, respectively. The energy levels are above 5% at all time.

E. Computation Complexity Analysis

To facilitate the broader application of the proposed framework by practitioners, the computation complexity of the proposed framework is analyzed across scenarios of varying scales, different inspection time and fleet sizes. Specifically, the computation time mainly consists of three parts: (I) the local planning for GCS, including the coordination of communication events and the rolling assignment of BBoxes; (II) the local planning for explorers, involving the $\texttt{FF3E}(\cdot)$ for exploration, the planning via $\texttt{SOEI}(\cdot)$ and the predictor of completion time; (III) the local planning for inspectors, encompassing the update of local plan $\{\xi_j^+\}$.

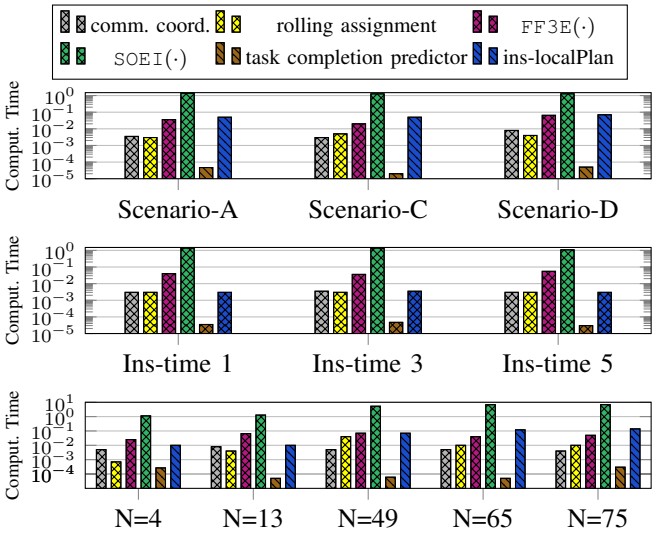

Figure 24: Computation time of main components of the proposed method: for three scenarios (**Top**); change of computation time under different inspection time in Scenario-C (**Middle**); with different fleet sizes in Scenario-A (**Bottom**).

To begin with, the computation time of each step above is analyzed in different scenarios, where 1 GCS, 4 explorers and 8 inspectors are deployed in three scenarios from Fig. 9 under inspection time $t_q = 3s$. As summarized in Fig. 24, all modules except the $\texttt{SOEI}(\cdot)$ for the explorers, take less than $0.1s$ across all scenarios. The $\texttt{SOEI}(\cdot)$ algorithm, which relies on an iterative optimization process, dominates the computation time of the local planning of GCS. Nonetheless, the total computation time of each step is less than $1.3s$ on average. Second, the same analysis is examined for different inspection time t_q, i.e., $1s$, $3s$, and $5s$ in Scenario-C with 1 GCS, 4 explorers and 8 inspectors. It shows that the inspection time slightly affects the computation time of $\texttt{SOEI}(\cdot)$module, but the overall computation time of each step is less than $0.25s$ on average. The same analysis is performed across different fleet sizes, i.e., 4 (1 GCS, 1 explorer, 2 inspectors), 13 (1 GCS, 4 explorers, 8 inspectors), 49 (1 GCS, 8 explorers, 40 inspectors), 65 (5 GCS, 10 explorers, 50 inspectors), and 75 (5 GCS, 10 explorer, 60 inspectors) in Scenario-A. It shows that the computation time grows steadily as the fleet size increases, ranging from $0.13s$ to $6.91s$ on average, as the planning requires more interactions to converge when the number of explorers and inspectors increases. Nonetheless, the overall computation for $N = 75$ remains below $8.82s$, showcasing its scalability to large-scale robotic fleets.

F. Hardware Experiments

1) Experimental Setup: Hardware experiments are also conducted to validate the practical feasibility of the proposed framework. As shown in Fig. 25, there is a $5m \times 5m \times 3m$ arena containing two mini-nature 3D structures, a T-shape structure of size $1.8m \times 0.3m \times 1.9m$ and a rectangular structure of size $0.5m \times 0.5m \times 2.0m$. In total, 9 features of interest as cracks are printed at unknown locations on their surfaces. Moreover, two "Tello" UAVs [51] equipped with monocular cameras serve as explorers, to perform exploration via 3D reconstruction. These explorers navigate at the speed of $0.7m/s$

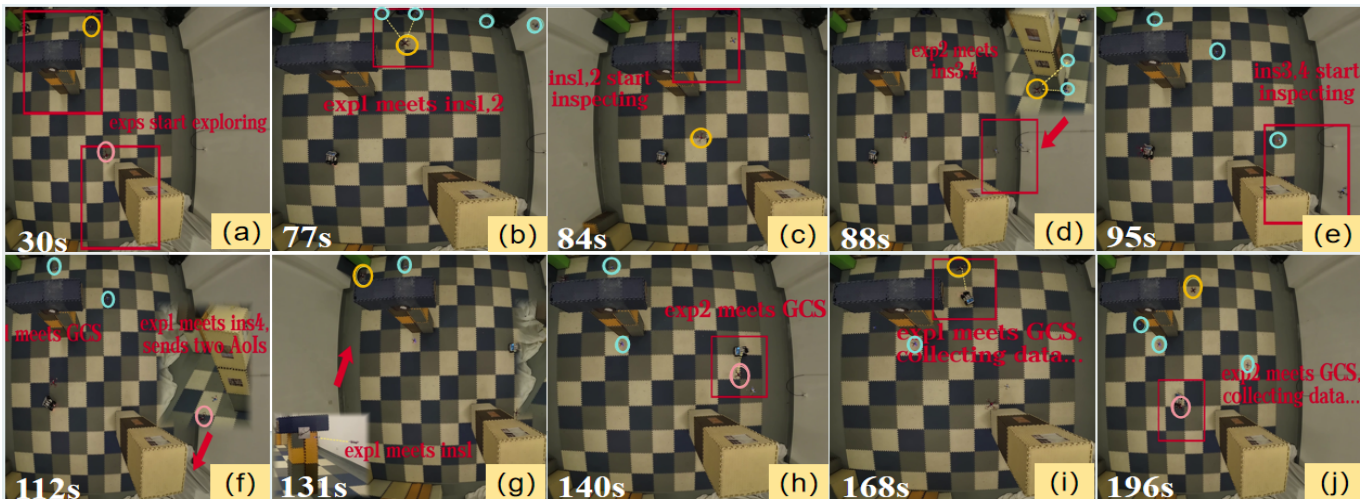

Figure 25: Snapshots of the hardware experiments involving 2 explorers (marked by yellow and pink circles), 4 inspectors (marked by indigo circles), and 1 GCS for the collaborative inspection of 2 structures and 9 AoIs. **(a)**: The explorers initiate the exploration; **(b)**: Explorer 1 identifies 2 AoIs and coordinates with inspectors 1&2; **(c)**: AoIs are allocated to inspectors 1&2; **(d)**: Explorer 2 detects 2 additional AoIs and coordinates with inspectors 3&4; **(e)**: AoIs are allocated to inspectors 3&4 to start inspecting; **(f)**: Explorer 1 initiates its first data transmission to the GCS; **(g)**: Explorer 1 discovers another AoI and coordinates with inspector 1; **(h)**: Explorer 2 establishes its first GCS communication; **(i)**: Explorer 1 transmits the inspected features and subsequent meetings to the GCS; **(j)**: Explorer 2 transmits the inspected features and subsequent meetings to the GCS.

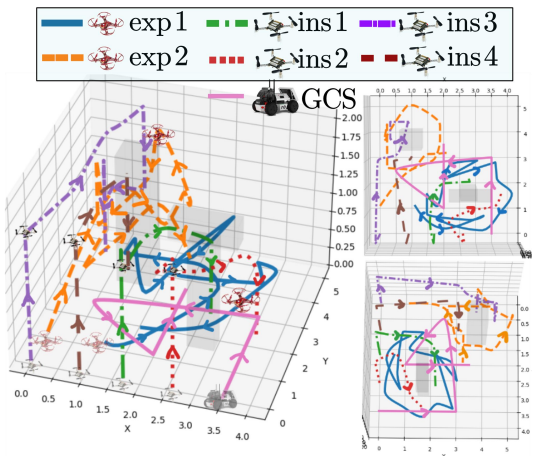

Figure 26: Complete trajectories of all 8 robots over the mission duration of $200s$, with arrows indicating the timeline in different of views: Front view (**left**), top view (**right-top**), and side view (**right-bottom**).

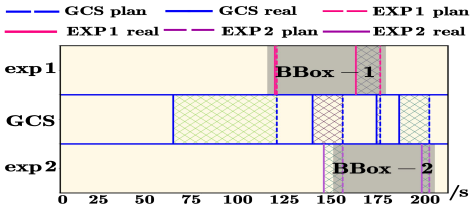

Figure 27: The planned and actual meeting events between the GCS and two explorers in the hardware experiments. The planned meeting time for the GCS (blue dashed lines) aligns with the explorers (pink and purple dashed lines), indicating the confirmed meeting event and the target BBox.

with a kinodynamic planner for obstacle avoidance and the communication range of $0.4m$. In addition, four "Crazyflie" drones [52] operate as inspectors at $0.3m/s$, employing an improved A* algorithm with priority-based collision avoidance and a communication range of $0.2m$. The AoIs on the surfaces are identified via the YOLOv7 package, the semantic segmentation module guides the FOV of the explorers towards to the target buildings, and reconstruction of the 3D environment by fusing RGB images with estimated depth information, which is predicted from monocular images of "Tello" using the MiDas network [53]. Lastly, one "LIMO" [54] four-differential ground robot acts as the moveable GCS, utilizing a EAI XL2 LiDAR for the real-time mapping and the `move_base` package for autonomous navigation. All robots are tracked by an OptiTrack motion capture system with 20 infrared cameras for positioning data, while all inter-robot communications are strictly limited to Line-of-Sight (LOS) constraints. It should be noted that the communication constraints among the robots are enforced centrally via a central node, including the relative distance, obstacle occlusion and bandwidth.

2) Results: The hardware experiment validates the performance of the proposed framework during the $200s$ mission. As shown in Fig. 25, 2 explorers initiate the exploration at $t = 30s$, as marked by red boxes in Fig. 25(a). Explorer 1 identifies 2 AoIs that might contain cracks by $t = 77s$ and coordinates with inspectors 1&2 through subsequent communication meetings as shown in Fig. 25(b). The AoIs are allocated following the `SOEI` algorithm, which directs the inspectors to their respective regions in Fig. 25(c). Simultaneously, explorer 2 detects 2 additional AoIs at $t = 88s$ in Fig. 25(d) and coordinates with inspectors 3&4 in Figs. 25(e-f). Concurrently, explorer 1 initiates its first data transmission to the movable GCS at $t = 112s$ in Fig. 25(f), including the inspected features and the subsequent meetings. At $t = 131s$, explorer 1 discovers another AoI and coordinates with inspector 1, while explorer 2 establishes its first GCS communication at $t = 140s$ in Fig. 25(h). Both explorers strictly follow the confirmed meeting events, with the last communication to GCS at $t = 168s$ and $t = 196s$ shown in Figs. 25(i-j). By

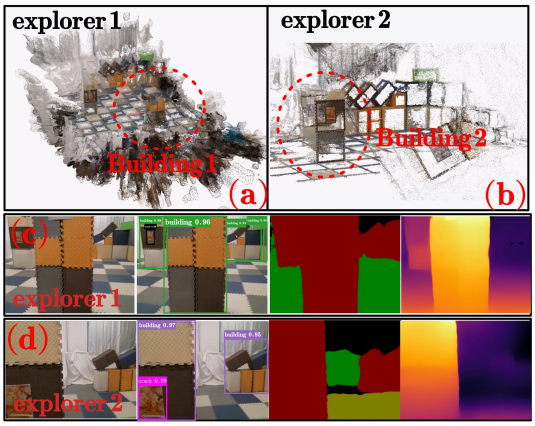

Figure 28: Perception results in the 3D environment via 2 explorers with the monocular cameras, including: re-constructed 3D environment for explorer 1((**a**)) and explorer 2((**b**)), recognition results of the AoIs and building structures with the raw camera images, AoI detection, semantic segmentation and depth estimation for explorer 1 ((**c**)), and explorer 2 ((**d**)).

then, all 3D structures and inspected AoIs are available at the GCS. Furthermore, the trajectories of all robots are recorded in Fig. 26, which indicate that (i) the explorers achieve a complete coverage and all AoIs are successfully inspected, as shown in Fig. 28; (ii) the GCS coordinates with both explorers for the optimal meeting events at four locations, as shown in Fig. 27; and (iii) all robots are collision-free with other robots and the 3D structures. Lastly, the detailed evolution of robot status within the first subgroup is summarized in Fig. 29, which validates the robustness of the proposed scheme under fluctuations in navigation time due to motion uncertainties and collision avoidance. Detailed videos of the hardware experiments can be found in the supplementary material.

VI. Conclusion

This work tackles the challenge of simultaneous exploration, inspection, and communication in large-scale, unknown 3D environments, via heterogeneous robotic fleets under limited communication. The proposed framework SLEI3D employs a multi-layer and multi-rate strategy, dividing the fleet into subgroups based on sensing capabilities, explorers equipped with long-range sensors identify areas of interest (AoIs), while inspectors with close-range sensors inspect the features. A ground control station (GCS) allocates tasks and facilitates communication using an intermittent protocol between the GCS and explorers, and a proactive protocol between explorers and inspectors to streamline task allocation and data collection. Extensive simulations validate its scalability and applicability to diverse scenarios and large-scale robotic fleets.

Future work includes: (I) enhancing the exploration efficiency of subgroups by enabling multi-robot exploration, which necessitates more sophisticated communication protocols; (II) developing exploration strategies that are independent of prior information, such as bounding boxes; (III) incorporating diverse feature types and inspector roles to handle more complex task requirements; (IV) integrating more realistic communication models, including Non-Line-of-Sight

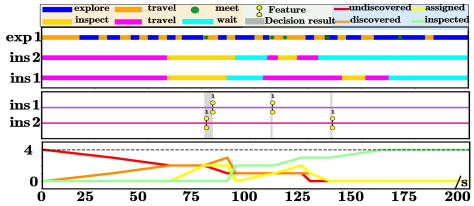

Figure 29: Top: Evolution of the robot status within one subgroup; **Middle**: Planning results during the meeting events between the explorer 1 and the inspectors 1 and 2; **Bottom**: Evolution of number of features being discovered, assigned and inspected over time.

(NLOS), signal attenuation, and multi-path effects, to enhance the system's robustness for real-world complex environments.

References

[1] M. Hinostroza and Lekkas, "Autonomous inspection and maintenance operations employing multi-robots: Preliminary results," in *Proc. IEEE/ASME Int. Conf. Mechatronic Embed. Syst. Appl. (MESA)*, 2024, pp. 1–8.

[2] J. Jiang *et al.*, "Key structure and technology of bridge cable maintenance robot–a review," *Robotic Intelligence and Automation*, vol. 45, no. 1, pp. 121–143, 2025.

[3] M. Afrazi and K. Lee, "The use of robotics in tunnel inspection and maintenance: A comprehensive review," *Advancements in Underground Infrastructures*, pp. 1–24, 2025.

[4] G. Best *et al.*, "Multi-robot, multi-sensor exploration of multifarious environments with full mission aerial autonomy," *Int. J. Robot. Res. (IJRR)*, vol. 43, no. 4, pp. 485–512, 2024.

[5] B. Yamauchi, "A frontier-based approach for autonomous exploration," in *Proc.Int.Conf.Robot.Autom.(ICRA)*, 1997, pp. 146–151.

[6] M. Naazare, F. G. Rosas, and D. Schulz, "Online next-best-view planner for 3d-exploration and inspection with a mobile manipulator robot," *IEEE Robot. Autom. Lett.*, vol. 7, no. 2, pp. 3779–3786, 2022.

[7] M. Allan *et al.*, "Planetary rover simulation for lunar exploration missions," in *Proc. IEEE Aerosp. Conf.*, 2019, pp. 1–19.

[8] M. S. Couceiro, "An overview of swarm robotics for search and rescue applications," *Artificial Intelligence: Concepts, Methodologies, Tools, and Applications*, pp. 1522–1561, 2017.

[9] M. L. Brutto, A. Borruso, and A. D'argenio, "Uav systems for photogrammetric data acquisition of archaeological sites," *Int. J. Heritage Digit. Era*, vol. 1, no. 1, pp. 7–13, 2012.

[10] P. P. Ray, "Internet of robotic things: concept, technologies, and challenges," *IEEE access*, vol. 4, pp. 9489–9500, 2016.

[11] G. Hu, W. P. Tay, and Y. Wen, "Cloud robotics: architecture, challenges and applications," *IEEE network*, vol. 26, no. 3, pp. 21–28, 2012.

[12] T. Murayama and A. Iwasaki, "Bi-connectivity control for multi-robot network considering line-of-sight communication," *J. Robot. Mechatron.*, vol. 35, no. 4, pp. 1028–1037, 2023.

[13] A. R. Mosteo, "Multi-robot task allocation for service robotics: from unlimited to limited communication range," Ph.D. dissertation, Universidad de Zaragoza, 2010.

[14] M. Guo and M. M. Zavlanos, "Multirobot data gathering under buffer constraints and intermittent communication," *IEEE Trans. Robotics (TRO)*, vol. 34, no. 4, pp. 1082–1097, 2018.

[15] K. Milidonis *et al.*, "Unmanned aerial vehicles (uavs) in the planning, operation and maintenance of concentrating solar thermal systems: A review," *Solar Energy*, vol. 254, pp. 182–194, 2023.

[16] Z. Tian *et al.*, "ihero: Interactive human-oriented exploration and supervision under scarce communication," *arXiv preprint arXiv:2405.12571*, 2024.

[17] S. Sharma and R. Tiwari, "A survey on multi robots area exploration techniques and algorithms," in *Proc. Int. Conf. Comput. Techn. Inf. Commun. Technol. (ICCTIC)*. IEEE, 2016, pp. 151–158.

[18] X. Hu and H. Pei, "A review of coordinated multi-robot exploration," in *J. Phys. Conf. Ser.*, vol. 2798, no. 1, 2024, p. 012037.

[19] A. Hussein *et al.*, "Multi-robot task allocation for search and rescue missions," in *J. Phys. Conf. Ser.*, vol. 570, no. 5, 2014, p. 052006.

[20] B. Zhou *et al.*, "Racer: Rapid collaborative exploration with a decentralized multi-uav system," *IEEE Trans. Robotics(T-RO)*, vol. 39, no. 3, pp. 1816–1835, 2023.

[21] R. G. Colares and L. Chaimowicz, "The next frontier: Combining information gain and distance cost for decentralized multi-robot exploration," in *Proc.ACM.Symp.Appl.Comput.*, 2016, pp. 268–274.

[22] Q. Dong *et al.*, "Fast and communication-efficient multi-uav exploration via voronoi partition on dynamic topological graph," *arXiv preprint arXiv:2408.05808*, 2024.

[23] F. Cabrera-Mora and J. Xiao, "A flooding algorithm for multirobot exploration," *IEEE Trans. Syst., Man, Cybern.*, vol. 42, no. 3, pp. 850–863, 2012.

[24] D. P. Doolittle, *Population Genetics: Basic Principles*. Springer Science & Business Media, 2012, vol. 16.

[25] G. Battocletti *et al.*, "Rl-based path planning for autonomous aerial vehicles in unknown environments," in *AIAA AVIATION 2021 FORUM*, 2021, p. 3016.

[26] F. Amigoni *et al.*, "Multirobot exploration of communication-restricted environments: A survey," *IEEE Intell. Syst.*, vol. 32, no. 6, pp. 48–57, 2017.

[27] M. N. Rooker and A. Birk, "Multi-robot exploration under the constraints of wireless networking," *Control Eng. Pract.*, vol. 15, no. 4, pp. 435–445, 2007.

[28] M. Saboia *et al.*, "Achord: Communication-aware multi-robot coordination with intermittent connectivity," *IEEE Robot. Autom. Lett.*, vol. 7, no. 4, pp. 10 184–10 191, 2022.

[29] C. Feng *et al.*, "Fc-planner: A skeleton-guided planning framework for fast aerial coverage of complex 3d scenes," in *Proc. Int. Conf. Robot. Autom. (ICRA)*, 2024, pp. 8686–8692.

[30] W. Jing *et al.*, "Coverage path planning using path primitive sampling and primitive coverage graph for visual inspection," in *Proc. Int. Conf. Intell. Robot. Syst. (IROS)*, 2019, pp. 1472–1479.

[31] ——, "Sampling based view planning for 3d visual coverage task with unmanned aerial vehicle. in 2016 ieee," in *Proc. Int. Conf. Intell. Robot. Syst. (IROS)*, vol. 1815, 1808, p. 2016.

[32] ——, "Multi-uav coverage path planning for the inspection of large and complex structures," in *Proc. Int. Conf. Intell. Robot. Syst. (IROS)*, 2020, pp. 1480–1486.

[33] M. Zhang *et al.*, "Soar: Simultaneous exploration and photographing with heterogeneous uavs for fast autonomous reconstruction," *arXiv preprint arXiv:2409.02738*, 2024.

[34] X. Xu *et al.*, "A cost-effective cooperative exploration and inspection strategy for heterogeneous aerial system," *arXiv preprint arXiv:2403.01225*, 2024.

[35] W. Sheng *et al.*, "Multi-robot area exploration with limited-range communications," in *Proc. Int. Conf. Intell. Robot. Syst. (IROS)*, 2004, pp. 1414–1419.

[36] A. R. Mosteo *et al.*, "Multi-robot routing under limited communication range," in *Proc. Int. Conf. Robot. Autom. (ICRA)*, 2008, pp. 1531–1536.

[37] M. Santos and M. Egerstedt, "Coverage control for multi-robot teams with heterogeneous sensing capabilities using limited communications," in *Proc. Int. Conf. Intell. Robot. Syst. (IROS)*, 2018, pp. 5313–5319.

[38] Y. Gao *et al.*, "Meeting-merging-mission: A multi-robot coordinate framework for large-scale communication-limited exploration," in *Proc. Int. Conf. Intell. Robot. Syst. (IROS)*, 2022, pp. 13 700–13 707.

[39] H. Khalil, *Nonlinear systems; 3rd ed.* Upper Saddle River, NJ: Prentice Hall, 2002.

[40] A. Hornung *et al.*, "Octomap: An efficient probabilistic 3d mapping framework based on octrees," *Auton. robots*, vol. 34, pp. 189–206, 2013.

[41] H. Chen *et al.*, "An improved deeplabv3+ lightweight network for remote-sensing image semantic segmentation," *Complex & Intelligent Systems*, vol. 10, no. 2, pp. 2839–2849, 2024.

[42] C.-Y. Wang *et al.*, "Yolov7: Trainable bag-of-freebies sets new state-of-the-art for real-time object detectors," in *Proc. IEEE/CVF Conf. Comput. Vis. Pattern Recognit. (CVPR)*, 2023, pp. 7464–7475.

[43] B. Zhou *et al.*, "Fuel: Fast uav exploration using incremental frontier structure and hierarchical planning," *IEEE Robot. Autom. Lett.*, vol. 6, no. 2, pp. 779–786, 2021.

[44] B. Alhijawi and A. Awajan, "Genetic algorithms: Theory, genetic operators, solutions, and applications," *Evol. Intell.*, vol. 17, no. 3, pp. 1245–1256, 2024.

[45] "Marsim." [Online]. Available: https://github.com/hku-mars/MARSIM.

[46] "Fuel." [Online]. Available: https://github.com/HKUST-Aerial-Robotics/FUEL.

[47] L. Han *et al.*, "Fiesta: Fast incremental euclidean distance fields for online motion planning of aerial robots," in *Proc. Int. Conf. Intell. Robot. Syst. (IROS)*, 2019, pp. 4423–4430.

[48] C. Wang *et al.*, "Multi-robot system for cooperative exploration in unknown environments: A survey," *arXiv preprint arXiv:2503.07278*, 2025.

[49] S. Zhu *et al.*, "Maexp: A generic platform for rl-based multi-agent exploration," in *Proc. Int. Conf. Robot. Autom. (ICRA)*, 2024, pp. 5155–5161.

[50] J. Chen *et al.*, "Meta-reinforcement learning based cooperative surface inspection of 3d uncertain structures using multi-robot systems," in *Proc. Int. Conf. Robot. Autom. (ICRA)*, 2024, pp. 7201–7207.

[51] "Tello." [Online]. Available: https://www.ryzerobotics.com/cn/tello.

[52] "Crazyflie." [Online]. Available: https://www.bitcraze.io/products/old-products/crazyflie-2-1/.

[53] R. Birkl *et al.*, "Midas v3.1 – a model zoo for robust monocular relative depth estimation," *arXiv preprint arXiv:2307.14460*, 2023.

[54] "Limo." [Online]. Available: https://www.agilex.ai/education/4.

Junfeng Chen received the M.Sc. degree (2019) in aircraft design from the School of Aeronautics Science and Engineering, Beihang University, China. He is currently pursuing the Ph.D. degree with the School of Advanced Manufacturing and Robotics, Peking University, China. His research interests include multi-robot systems, task planning, LLMs and robot learning.

Yuxiao Zhu is currently a junior pursuing a B.S. in Applied Mathematics and Computer Science at Duke Kunshan University, China. His research focuses on leveraging large language models (LLMs) to enhance task allocation and online adaptation in heterogeneous multi-robot fleets.

Xintong Zhang is currently a junior student pursuing a B.S. degree in Applied Mathematics and Computer Science at Duke Kunshan University, China. Her research interests focus on adaptive coordination and communication in multi-robot systems, particularly under challenging conditions.

Bing Luo received the PhD degree from the Department of Electrical and Electronic Engineering, University of Melbourne (UNIMELB), Australia, in 2020. He is now an Assistant Professor with Duke Kunshan University, and an Honorary Assistant Professor at Hong Kong University. Before pursuing his PhD degree, he was a project manager at China Mobile Corporation. His research interests are federated and edge learning, multi-agent system, and network optimization. He was the recipient of the 2018-2019 UNIMELB Kenneth Myers Memorial Scholarship (one recipient every two years), the 2017 UNIMELB Robert Bage Memorial Scholarship, the 2015 China Mobile Technical Innovation Award, and also held the 2026 Visiting Fellowships at Clare Hall, Cambridge University.

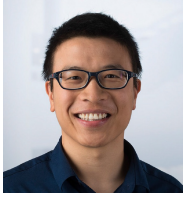

Meng Guo (M'11) received the M.Sc. degree (2011) in System, Control, and Robotics and the Ph.D. degree (2016) in Electrical Engineering from KTH Royal Institute of Technology, Sweden. He was a postdoctoral associate with the Department of Mechanical Engineering and Materials Science, Duke University, USA. During 2018-2021, he worked as a senior research scientist on Reinforcement Learning and Planning at the Bosch Center for Artificial Intelligence (BCAI), Germany. Since 2022, he is an assistant professor at the School of Advanced Manufacturing and Robotics, Peking University, China. His main research interests include task and motion planning for robotic systems.